# Using Geophysical Tools to Resolve Areas of Seismic Ambiguity

Farin Wilson

A report prepared in partial fulfillment of
the requirements for the degree of

Master of Science
Earth and Space Sciences: Applied Geosciences

University of Washington

June, 2014

Project mentor:
Rebecca Saltzer, ExxonMobil Development Company

Internship coordinator:
Kathy Troost

Reading committee:
Mike Brown
Juliet Crider

MESSAGe Technical Report Number: 010

## Abstract:

The flanks of an oil-bearing structure were investigated to determine the most likely reservoir geometry in an area where the seismic path forks in preparation for a field equity redetermination. Two alternate hypotheses were evaluated: a “high fork model” where the reservoir top follows the higher of the two paths and a “low fork model” in which the reservoir follows the lower path. I took four approaches to evaluate the hypotheses: 1) Depth conversion by multiple velocity models to evaluate the fidelity of the picked horizon on models that did not contain a fork; 2) hand interpretation around the areas of high uncertainty to eliminate their influence; 3) path choice effects on the plausibility of the environment of deposition; and subsurface geometry modeling with synthetics to compare calculated 1D seismic responses with current data. Investigation established that both fork interpretations cannot follow a continuous seismic reflector but are otherwise equally plausible. Interval modeling revealed several structure scenarios, supporting both high and low fork, which fit the seismic data. To augment the lower fork argument, a scenario with an additional sand interval off-structure is recommended, for simplicity and reasonability.

Note: To protect the proprietary interest of the internship sponsor, all numbers have been rounded and identifying details have been slightly modified or omitted. Definitions for italicized words can be found in the glossary.

## Table of Contents

## List of Figures

## List of Tables

## Acknowledgements

Supervisor, Steve Woods
Mentor, Rebecca Saltzer
The Celo team at ExxonMobil
My advisors, Juliet Crider and Kathy Troost
My fellow MESSAGe students
The ExxonMobil Development Company for the internship opportunity

## Introduction

The work completed investigating Celo field was to support ExxonMobil in an equity redetermination process. Seven companies hold interest in the field. When the discovery was first made, a preliminary cost/revenue split was agreed upon, with a reevaluation set for 2014. Five additional wells have since been drilled and new seismic data has been acquired. In April 2014, each of the seven companies delivered new estimates of the amount of hydrocarbons present on their lease blocks (equity), based on their own research and proprietary data acquisition. If the proposals (after eliminating up to 2 outliers) agree within 2%, the final determination of equity is based on the average of the remaining proposals. If the remaining proposals do not agree within 2%, there will be a 30-day negotiation phase. The companies can either independently come to an agreement during this phase, or each company will submit their technical case to an outside expert. Any expert decision will be pendulum: the numbers associated with the case judged to be most technically sound will be final and there will be no averages. The equity percentages will not be based on traditional pore-space measurements, but on net rock volume. There are options for additional redeterminations in the future, as the field goes into production and more data becomes available.

The focus of my internship was on helping to build a solid technical argument that could be used if the redetermination were to be deferred to an outside expert. The position of the top of the main reservoir on the flanks of the field appears to fork in seismic data, and can be interpreted to follow either the high or low reflector. The reflector chosen impacts the overall net rock volume calculations and must be technically justified to expert scrutiny. I investigated the basis for both high and low forks through seismic horizon interpretation, isochore analysis, depositional evidence, and rock property modeling.

## Field Background

This study evaluates a seismic reflector fork in the Celo Field in the Gulf of Mexico. Investigative work regarding the nature of the field has been completed by ExxonMobil and partners; references for field background information can be found in internal ExxonMobil reports (ExxonMobil, 2012). The Celo field is thought to have an environment of deposition on the edge of a prograding fan complex (figure 1, Reading and Richards, 1994). The age intervals of sedimentary units range from Tortonian to Calabrian; the reservoir of highest interest is late Pliocene (figure 2, Walker et al. 2012).

This field is a *deep-water* reservoir at 7000 feet below sea level and is *subsalt* with as much as 9000 feet of salt above the horizon of interest. The shape is a half dome (figures 3-4, Visual Logic, 2014), truncated by a large fault just west of the crest. The northern segment of the fault juxtaposes sediment above salt; the southern segment of the fault juxtaposes two sedimentary sequences. Separated from the Celo Field by the faults, the area to the west contains Ammon, a similar field

currently moving into production. The fields have roughly the same intervals, but the Celo field is 2000 feet deeper due to faulting.

There are currently nine wells on site, several with multiple *sidetracks*. Because of pressure-related safety concerns, several wells were not completed at the intended depth. Nearly all wells are on the crest of the structure (figure 5). Well data includes: seismic velocities, electrical resistivity, density, gamma ray, and thermal neutron porosity. An interpreted percentage of shale and calculated *synthetics* are also available and presented below.

Figure 6 shows a hand-drawn well log representative of the area showing the percentage of shale and an 18 Hz synthetic. The intervals as picked by ExxonMobil Formation Evaluation Specialists are described below with their abbreviations. Net to gross (NTG) refers to the proportion of the interval that contains petroleum-bearing rocks.

G:MS Thin intermittent interval of minor sands (G: **M***inor* **S***ands*)

F:SH Shale (F: **SH***ale*)

E1:CS, E2:CS
70% NTG highly channelized sands, separated by a thin shale
(E1:**C***hannel* **S***ands*, E2:**CS**)

D:CO *Debrites*, shales, highly variable cutoff (D: **C***ut* **O***ff*)

C:TB Thin beds of shale and sand with inconsistent proportions (C: **T***hin* **B***eds*)

B:MR *Main Reservoir*
>95% NTG 100' blocky massive sands punctuated with 10' marls, high porosity
(B: **M***ain* **R***es*)

A:LC Sands with volcanics, clastics, extensive lateral compartmentalization
(A: **L***ateral* **C***ompartmentalization*) (not shown)

In general, the reservoir is in the sand units. The sands, in comparison to surrounding shales, generally display decreases in velocity, neutron porosity, density, and resistivity as measured on the well logs. The sands are also low impedance (impedance is the product of density and velocity). A *zero-phase synthetic* indicates a change to sands with a *trough*. The Celo units generally thicken away from the crest (off-structure).

## Data Background

The interpretation of reservoir volumes is conducted with three-dimensional seismic reflection data. Seismic volumes are three-dimensional representations of the subsurface geology. Accurate representations rely on careful determination of the velocity of seismic waves through the rocks of interest. For this project, several models of the subsurface velocities (velocity models) exist: The multiple seismic volumes available represent one data collection event that has been processed with several different velocity models. The initial seismic data was reprocessed with interactive ExxonMobil expert feedback in 2011 and 2013, (VM1 and VM2 volumes, based on velocity models 1 and 2) but both were mainly focused on a field to the far east, East Ammon. Stratigraphy and velocity assumptions from East and West Ammon were carried over to Celo field. Care was taken to ensure agreement with existing Celo field well data.

Also delivered in late 2013 was a reprocessing effort that used a salt flood and full waveform inversion (FWI) in the shallow sediments, VM3 (from velocity model 3). A salt flood is a technique used to locate the base of salt. The seismic data is processed with a velocity model that assumes everything below the top of salt is a salt velocity. Where the subsurface changes from the base of the salt to sediment shows up as an anomalously strong reflector. This salt edge is then incorporated into future models. FWI starts with a basic velocity model based on broad predictions. It applies the model to the *gathers*, then focuses on the areas where the velocity model is obviously insufficient. The areas of misfit are analyzed and the model is updated. This process can repeat many times. The resulting velocity model should be much higher-resolution (figure 7, Chao et al. 2014).

This FWI effort was focused on East Ammon field but was *migrated up to 40 Hz*, much higher than the standard 15 Hz. Because Celo field was not the main focus of the reprocessing, VM2 and VM3 includes areas of atypical velocities in order to match, or 'tie' the well data. Polygon-like areas of high or low velocities are present above the reservoir. While not necessarily directly representative of the substrate, when the seismic data (natively in time) is converted to depths with velocity models, the result at the reservoir agrees with the depth from the well data.

The effects of different velocity models on the area of interest are significant. One major difference is the speed of the salt - some models treat it as 'clean' (~15,000 feet per second (fps)) while in others the salt is 'dirty', intermixed with sediments (~12,000 fps, highly location dependent). A small change in the velocity model can easily change the thickness, angle, depth, connectivity, and oil-water contact (OWC) of a reservoir.

For this field, the main velocity model used for interpretation has been VM1 (figure 8). While the other velocity models are valuable and offer insight into possible solutions, they were not delivered until late 2013, midway through the work on the equity redetermination process.

## Project Area

The focus of this project is on the flanks of the main reservoir. Just above the OWC, the top of the interval appears to fork in the VM1 seismic (figure 9, Huuse, 2008). That is, based on reflectors in VM1, there are two possible interpretations for the position of the top of the main reservoir. The amount of net rock volume between the forks is minor compared to the total reservoir, but the decision affects the placement of the OWC and must be technically justified if the equity case goes to an expert decision.

Interpreting the reservoir on the low fork of the reflector moves the OWC in map view more than 1000 feet to the west, a noticeable shift (figure 10).

The upper, or highfork, option has a higher seismic reflector amplitude than the lower fork. The distance between the reflectors is ~120'. The seismic resolution in the area is about 15 Hz, with a resolution of about 130' in sands (Appendix equation 1, Rafaelsen, 2014). Prior to this project, the team working the reservoir has interpreted the horizon to follow the lowfork. A co-venture company in the Celo field has interpreted the horizon to follow the highfork. My goal is to examine the basis and implications of both paths to determine plausibility and possible geologic settings.

## Seismic Interpretation

While the reservoir wasn't interpreted on the seismic data processed with any velocity models other than VM1, these other models may be used to help resolve some of the ambiguity. The velocity model cubes are initially in-depth: the absolute velocity of each body (stratigraphic interval) is portrayed at the theorized depth (figure 11A). Each interval/depth velocity model is converted into an average/time model using Petrel software (Schlumberger, 2012). This new model calculates the average velocity of each gather through time (figure 11B). A gather may be going an average of 6000 fps through shallow sand for 15s, then encounter 15,000 fps salt, increasing the average to 10,000 fps at 20s, 14,000 fps at 40s, etc.

The z-units of VM1 seismic data can be converted from depth to time by applying a model using VM1's average velocity cube. This time is considered 'raw data' and can be run through models with VM2, VM3, or a co-venture's average velocity cube to change the z-units back to depth. An interpreted horizon can go through the same process to generate a depth-converted representation of the horizon on many different models (Fig 11C).

The traces that made up the reflector of the horizon of interest in VM1 have now been vertically shifted according to the new velocity models. The goal was to evaluate the placement and relative amplitude of the horizon of interest on seismic models that did not contain a fork. The result of the depth conversions was not as smooth as expected, but was vacillating around the reflectors (figure 12). These jitters occurred in every depth conversion across four velocity models at approximately the same places. The location of the worst jitters were outlined as polygons of seismic

accuracy uncertainty (figure 13). They roughly correspond to the area where the horizon of interest forks in VM1.

These type of depth conversions are a 1D vertical process, and the software does not take into consideration 3D migration. Because there appear to be problems across all velocity models in slightly different areas, I interpret the cause not to be isolated to the initial model. Looking closely at the average velocity cubes, in some areas a slight 'striping' can be seen. These correspond to places where the average velocity is changing substantially over a short distance (figure 14). The cause of such large jumps can be traced to the widely varying depth of the top of the salt. In the area of the reservoir, the overall thickness of the salt varies more than 14,000'. These large variances in subsurface velocity produce significant edge effects that make any seismic data in that area unreliable. Even small changes in the position of the salt 'cliffs' significantly affect the resulting position of the velocity-migrated seismic reflectors.

The areas within the polygons of uncertainty need to be deemphasized when trying to resolve the flank-fork issue. The polygons create a somewhat continuous zone with relatively reliable data surrounding them. To mitigate the polygons' influence, I attempted a new interpretation on VM1, omitting the area of uncertainty. I based this interpretation off the core of the team interpretation near the crest (figure 15). Both *inlines* and *crosslines* were considered. The interpretation followed stretches of continuous reflectors, moving between inlines and crosslines. Every interpretation is somewhat subjective, depending on spacing of sampled lines, a continuous reflector on one inline might not be continuous or even follow the same trend on the next sampled inline. The interpretations also have areas where personal judgment and inference must be made. Four separate iterations following a continuous reflector around the areas of uncertainty were completed, each interpretation placed the top of reservoir B:MR on the highfork.

A fundamental problem with the resulting interpretations was that interpreted sedimentary contacts were found to cross reflectors. On close inspection, it was found that the original lowfork interpretation also has to cross reflectors. Several locations were discovered where both lowfork and highfork crossed reflectors, either on the inline or crossline (figure 16).

Another tool to evaluate the position of the top of the reservoir is an isochore, or true vertical thickness (TVT) map. The highfork interpretation thickens the flanks of the reservoir 120', thinning the above interval C:TB by 120'. Changing the unit thickness requires modification of the interpreted environment of deposition. A C:TB that thins on the flanks more closely represents a heavily channeled submarine valley, different from the previous environment of a moderately channelized basin floor. The environment of deposition for the main reservoir B:MR remains the edge of a lobe complex, but when thickened on the flanks it represents a steeper slope. Because both highfork and lowfork interpretations support reasonable environments of deposition, an isochore analysis cannot be used to rule either one out.

## Channel Investigation

While examining the interpretation, several possible channels were discovered on the top of interval B:MR (figure 17,Huuse, 2008). The channels were moderately continuous, but could not be followed with confidence for any useful length. They occurred in the same vicinity as the flank forking. To further investigate the channels, several types of seismic manipulation were attempted.

Full-volume skeletonization is a proprietary ExxonMobil Petrel software capability. It works by identifying small areas with topologically consistent reflector surfaces, attempting to merge these with nearby similar surfaces (figure 18D, Matthias, 2011). The program identifies and rejects surfaces that overlap, are not locally consistent, or globally consistent (figure 18 A, B, C, Matthias, 2011). The result is a three-dimensional, navigable, multi-surface model (figure 19, Matthias, 2011). Channels can often be easily identified in the final product. This technique is not useful in highly faulted areas - the program cannot infer continuous surfaces across the faults. An area surrounding the possible channels in the Celo reservoir was isolated and skeletonized. The result was inconclusive: while the number of faults in this zone were limited, they interfered with the created surfaces in crucial areas, making any channel visualization impossible.

A second option to investigate the location and existence of possible channels is multi-horizon flattening. This technique works by taking user-picked horizons and restoring them to the assumed original horizontal orientation. This structural restoration involves shifting the horizons in depth (to undo faulting), and squeezing or stretching the surrounding area (to undo folding or compaction). The final result is at least two parallel horizons with ideally visible, continuous, reflectors between them. In the Celo reservoir, multi-horizon flattening was completed using the tops of A:LC and E2:CS intervals. The product revealed irregular channel traces similar to those seen in the unflattened volume.

The last technique to be applied to the seismic data was spectral decomposition. Due to the depth of the reservoir, most of the high frequency waves have been attenuated and the low frequency waves dominate the response. At these depth, low frequencies have a much better signal to noise ratio. A frequency of 12 Hz was extracted from the VM1 seismic data, eliminating much of the noise and wavelet interference. The reflection resolution was ~205', adequate to identify the top of the B:MR reservoir along with any significant channels. Unfortunately, this attempt did not yield any additional concrete evidence to aid in the flank fork problem or to resolve the channel question. The sporadic nature of the 'channel' evidence combined with their proximity to the uncertain seismic area leaves any channel theory in serious doubt.

Despite depth conversions, multiple hand-interpretations, isochore analysis, flattening, and spectral decomposition, examinations of the seismic data have yielded no concrete answer regarding the most accurate path in the reservoir B:MR flank fork issue. The next step is to look deeper into

the mechanics of the seismic data to analyze what sort of scenarios could be causing the response seen.

## Geophysical Modeling

Well log data provides velocities, densities, and an interpreted shale percentage curve for all the intervals of interest in Celo field. Using the velocity and density, impedances for each interval in each well can be calculated and a corresponding synthetic seismic trace generated (see figure 6). With the RokDoc software (Ikon Science, 2014), a user can create structures, with each body having unique velocities and densities, and the software will calculate 1D convolutional synthetics along an inline, crossline, or arbitrary line. These seismic responses can be compared to the actual seismic data to determine possible structure and interval characteristics. Raw well data also can be imported and used to create crossplots, x-y scatterplots with rock properties on the axes. For my investigations, combinations of velocity, density, depth, impedance, and % shale were used. RokDoc is also capable of filtering the data being plotted; I used crossplots filtered by a low or high % shale to look at the properties of just the sands or shales in each interval.

For the Celo field, rock property analysis was completed using RokDoc and Matlab. Initial model values were based on the three closest wells to the inline (figure 20). The wells were parallel to the depth trend of the reservoir. Each interval has three distinct depths represented. Unfortunately for the analysis, there are no wells near the flank area. Interval depths in the well logs were previously identified by formation evaluation specialists. The section of interest, delineated as a single interval in the well logs, typically contains a mixture of the dominant formation and intermittent interbedding or inclusions of adjacent formations. To model solely the formations of interest, I include in the rock property analyses only data clearly associated with shale formations (shale > 80%) or sand formations (shale <30%). To achieve broadly representative values, the three well logs were combined and each interval's properties were plotted by depth (figure 21). If the estimated flank depth of the interval was represented in the cross plot, an average of those points was taken. If the estimated depth was below that of the cross plot, the average of the lowest point on the plot was used. I find that typical shale for the Celo field has seismic velocity of 9,300 fps and density of 2.3 g/cm$^3$, a typical water sand (sand with water in the pore spaces) is 8,600 fps and 2.15 g/cm$^3$. These numbers are within a reasonable range for the depths and similar to nearby fields. The initial values for each interval are shown in table 1.

The models tested were based off of possible geologic scenarios discussed with the Celo field team. The intervals in all the models are only modified from the seismic fork area to the flanks: they all tie to the available well data. Several intervals were subdivided based on well log information, D:CO and E1/E2:CS were combined for interpretation purposes but have been subdivided into D:CO, E1:CS and E2:CS. C:TB and B:MR intervals were also combined for interpretation purposes but are treated separately for the geophysical models. The tops of A:LC, E2:CS, and the base of salt (BOS) have been confidently interpreted on the VM1 seismic in the area modeled, their positions are

constrained. The delineation between D:CO and E1/E2:CS and between C:TB and B:MR must be estimated. The thicknesses of D:CO and C:TB were obtained from each of the 9 well logs and averaged. Outliers past one standard deviation were discarded (figures 22, 23). Because the estimated thicknesses were from wells in the crest area where the formations were dipping significantly more than on the flanks, each measurement was converted into true stratigraphic thickness (TST).

To build the base lowfork model, the picked horizons for BOS, E1/E2:CS, D:MR, A:LC and the base of A:LC were imported into Rokdoc. E1/E2:CS begins to thicken above the OWC. D:CO was calculated to be ~40% of E1/E2:CS thickness. The generated top of the D:CO surface continued this trend, going from ~100' at the crest to ~140' on the flank. To preserve TST, the dip angle of the formation was extracted from Petrel and incorporated into the thickness calculations (figure 24). For the base model the C:TB was kept at a constant 110'. Unlike D:CO, there is no obvious evidence in the well logs for a thickening of C:TB. The full view of the base model with labeled bodies is shown in figure 25.

Lowfork Base Model:

Using the selected rock properties, synthetic traces of a zero-phase 15 Hz wavelet are shown in the two figures below, with the full view and a zoomed view on the area of interest (figure 26). To help visualize why the synthetics respond as they do, figure 27 shows the zoomed view with relative impedances. Note the clear differences at the OWC. Figure 28 shows the synthetics with a sketched seismic overlay.

Looking at figure 26, the wavelet sidelobe energy can clearly be seen coming off of the trough between F:SH and E1/2:CS (A). The side lobes from C:TB /B:MR (B) work to diminish the TB and D:CO response while the C:TB/D:CO (C) side lobe amplifies E1/2:CS / D:CO (D). Below the OWC in the center area of interest, this model's synthetics are completely out of phase with the VM1 seismic data.

One geologic scenario explored to bring the modeled reflections into phase with the observed seismic waveforms was to thicken either the C:TB or D:CO. Three models were built and tested.

C:TB thicken 15% and C:TB thicken 50%:

The C:TB horizon from the base model was bulk shifted to replicate thickening by either 15% (from 110' to 126') or 50% (from 110' to 165'). The thickening trend started just above the OWC. Figure 29 shows synthetics with seismic overlay for a thickening of 15%. Only the area of interest, the zoom view, is shown.

Thickening the C:TB 15% is not enough spacing to generate a side lobe trough within the C:TB (A). The trough can be seen by increasing the C:TB to 50% (figure 30). A 50% thickening matches the seismic at the D:CO/C:TB (A) interface and below but not above.

Maximum D:CO thickness:

Instead of thickening as a percentage of E1/E2:CS, in this scenario, E1/E2:CS is a constant thickness and D:CO takes up all of the additional thickening. D:CO changes from 100' at the crest to 250' on the flank (figure 31).

This thickening allows the model to tie the seismic at the E1/E2:CS / D:CO (A) interface, but it does not correspond below. Thickening the D:CO works for the upper part of the model, while thickening the C:TB works for the lower. If both are incorporated into a single model, they would nearly match the existing seismic, but lacking an extra cycle within D:CO. With the current rock properties, another low impedance body must be added to the model.

Given the overall environment of deposition, an additional sand pulse off-structure is reasonable. Within the submarine fan, the sediment source creates new lobes over time, generating a lobe complex (Reading, 2009). While B:MR is close to the center of a lobe, the much thinner sand pulse visible on Celo Field would represent the edge of a nearby lobe. Two models were designed, one with the sand pulse on top of the C:TB and one with the pulse within D:CO.

Sand Pulse on top of the C:TB:

An extra interval of 50' of low NTG sand was placed on top of the C:TB downflank of the OWC. The top of D:CO was not adjusted. This effectively keeps D:CO at a constant thickness of 100' instead of thickening as a percentage of E1/E2:CS. Figure 32 shows just the basic bodies, figure 33 is with synthetics and seismic overlay.

The Sand Pulse has an impedance similar to C:TB; much of the peak seen near the interface is constructive interference of the side lobe energy from D:CO/sand pulse (A) and C:TB/B:MR (B). This model does not improve on the base mode. There is no match to the seismic data below the OWC.

Sand Pulse within D:CO:

A pulse of low NTG sand was hand-drawn to fit the seismic data within the D:CO interval. The top of D:CO is moved higher to keep the total D:CO volume constant with the base model. Figure 34 shows the zoom view, figure 35 is the synthetics with a seismic overlay and figure 36 is the synthetics with relative impedances.

Placing a low impedance pulse in the much higher impedance D:CO generates strong reflectors, creating a model that fits the seismic data. The additive properties of the side lobes of

E1/E2:CS / D:CO (A) and sand pulse / D:CO (lower) (B) help to boost the trough at sand pulse (upper)/D:CO (C). This allows the top of B:MR to have a lower amplitude response than the top of the sand pulse, a key feature in the seismic data.

Base High Fork model:

The same methods as the base Low Fork model were used to explore the highfork model, except that the top of the C:TB and base of D:CO now follow the High Fork interpretation, a maximum shift of 120' higher. The base of the C:TB remains the same. This significantly thins E1/E2:CS. Figure 37.

This model fits the seismic data with minimal alterations.

## Lateral Variations within Units

The initial models were created with basic rock property assumptions. Well placement and the structure of the field mean that there is no data available that corresponds to the formations at the flank depth. For the following two models, rock property depth trends were estimated and a lateral variation was applied to the models.

Given the irregularities within the D:CO unit, it is almost certainly laterally changing. Crossplots of the interval show a change from 7,000 fps to 12,000 fps across wells in less than a hundred feet. For this model, D:CO changes from a shale dominated to a sand dominated interval, supported by the trend seen in the wells along the modeled inline.

D:CO with lateral variation:

Figure 38 shows how using the low fork base model with D:CO lateral variation offers an additional method to match the seismic at the E1/2:CS / D:CO interface (A). In this model, on the far flanks D:CO is slower than the C:TB, creating a new mismatch with the seismic. Midflank, the impedance difference between E1/2:CS /D:CO (A) is negligible, with synthetics showing no reflectors. The flank fit at the top of D:CO is the first solution to fit this area without changing the base surface, but this model still has significant problems. More lateral variation is required.

The exact surfaces used in the team Petrel modeling and calculations were imported for the final model. An inner shale of 10' has been added between E1:CS and E2:CS sands. The shale is well below seismic resolution, but increases the specificity of the models. The properties of the salt and shales were not changed, they have no impact on the area of interest. All model fill values can be found in table 1, appendix.

All nine wells in the field were considered. If the interval trend was not consistent across the field, more weight was given to the three wells on the inline used for the models. In some cases, the observed increase in speed is more than what can be reasonably expected for depth alone. These intervals must have a rock type change as well (figure 39). E2:CS and especially E1:CS both appear to change from ~70% NTG to shales while D:CO undergoes very little impedance change, estimated to be from a combination of depth and increasing sand content.

Team surfaces with lateral variation:

The lateral variation accounts for the extra cycle within D:CO by using the side lobe energy of the now shaley E1:CS /D:CO interface (A) (figure 40). The changes in rock type are realistic with a prograding fan complex. In this model E1:CS and E2:CS are separate sand lobes, slightly offset; they both grade to less sand on their edges the flank of the inline modeled is closer to the edge of E1:CS's sand lobe. D:CO, the debritic cutoff, is known for its variability and a bulk change to sand is not unreasonable. Figure 41 shows how the relative impedances change down the flank. This model matches the seismic data.

Three tested geologic models fit the VM1 seismic data along the selected inline: highfork with thickened C:TB, lowfork with a sand pulse in D:CO, and lowfork team surfaces with lateral variation. For the purposes of an equity redetermination, the Sand Pulse model is recommended. The flank fork is a relatively minor issue in a complicated field, a simple and reasonable explanation with clear figures will present the expert with a logical solution supporting the team interpretation choice.

## Summary

The top of the reservoir in Celo field appears to fork near the flanks of the structure in the primary seismic volume. This fork is just above the OWC and the volume of hydrocarbons within the fork is a relatively small amount. However, as the reservoir is moved from the highfork to lowfork option, the movement of the OWC in map view is substantial. The field is currently going through an equity redetermination and needs to have a solid technical case for either fork choice that can be presented to an outside expert. It is known that not all companies going into the redetermination are in agreement as to the reservoir geometry.

Depth conversion of the top of the reservoir track through multiple velocity models revealed an abrupt change in the thickness of the salt above, co-located with the area of uncertainty. The edge effects of these salt 'cliffs' is creating areas of high uncertainty in the seismic data. To try and mitigate the edge effects, several interpretations circumventing the area were completed. Each interpretation found the highfork to be the likely solution based on seismic trace following. Both the high and lowfork choices have a fundamental problem: they cross reflectors multiple times. Neither can be conclusively defended based on interpretations alone.

Changing from the high to low fork has the potential to change the environment of deposition. Evaluating the subsequent change in thickness of the intervals showed that both options support a viable environment. Possible channels were also explored through interpretation, skeletonization, flattening, and spectral decomposition with the hope that they could give depositional indications. No potential channels could be followed to a high level of confidence.

Seismic interpretation techniques gave no conclusive answers as to the most correct option. The next step was to perform geophysical modeling, comparing the calculated synthetics for possible subsurface geometries to current seismic data. Rock properties were assigned from nearby well data. Base models were analyzed, along with the thickening of intervals and the addition of sand pulses. The highfork base model and a sand pulse model both created synthetics that approximated the known data. Because the only well data available is on the crest, several models were attempted, incorporating lateral variation to follow depth and proximity trends seen in the wells. A model using previously constructed team surfaces and extensive lateral variation was also found to generate synthetics that fit the seismic.

There is no conclusive evidence to support the high or lowfork decision. For purposes of presenting a lowfork technical case to an expert in an equity redistribution, a subsurface model with a simple sand pulse is recommended, for simplicity and reasonability.

## References

"Salt Domes." {LaB}. 03 Feb. 2010. Web. 03 May 2014. <http://lab.visual-logic.com/2010/02/salt-domes/>.

Huuse, Mads. "Virtual Seismic Atlas." Shallow Profile GR98-01. Virtual Seismic Atlas, 01 Feb. 2008. Web. 02 May 2014. <http://see-atlas.leeds.ac.uk/homePages/generic.jsp?resourceId=090000648000f1be>.

Ikon Science. RokDoc. Computer software. Vers. 6.1.2. N.p., 2014. Web. <http://www.ikonscience.com/rokdoc-software>.

Matthias, Imhof G. Seismic Horizon Skeletonization. Imhof Matthias G, assignee. Patent US 20110048731 A1. 3 Mar. 2011. Web. 02 May 2014. < http://www.faqs.org/patents/app/20130151161>.

Rafaelsen, Bjarne. "Seismic Resolution (and Frequency Filtering)." Svalex. University of Tromsø, 16 Aug. 2006. Web. 04 Mar. 2014. <http://folk.uio.no/hanakrem/svalex/E-learning/geophysics/Seismic_resolution.pdf>.

Reading, H. G., and Richards, M., 1994, Turbidite systems in deep-water basin margins classified by grain size and feeder system: AAPG Bulletin, v. 78, p. 792–822.

Reading, H. G., ed. Sedimentary environments: processes, facies and stratigraphy. John Wiley & Sons, 2009.

Schlumberger. Petrel E&P 2012.6. Computer software. N.p., n.d. Web. <http://www.slb.com/petrel>.

Walker, J.D., Geissman, J.W., Bowring, S.A., and Babcock, L.E., compilers, 2012, Geologic Time Scale v. 4.0: Geological Society of America, doi: 10.1130/2012.CTS004R3C. ©2012 The Geological Society of America. Web. 02 May 2014.

Wang, Chao, Anadarko, and Lumina. "Joint Multi-parameter Anisotropic Full Waveform Inversion with Randomized Shot Sampling." Northside Tech Breakfast. Houston. 04 Mar. 2014. GSH Meeting. Web. 03 May 2014. < http://www.gshtx.org/en/cev/1097>.

## Glossary

Debrite: poorly sorted, matrix-supported debris flow, without internal structure.

Deep-water: An oilfield with water depths over 600' (roughly deeper than typical continental shelves). (Schlumberger, 2014)

Inlines/crosslines: Inlines are lines parallel to the direction the seismic was acquired (e.g. towed array lines for marine applications). Crosslines are perpendicular.

Migration: Using a velocity model to move gathers from a raw time scale to a depth scale. The gathers can be filtered to a higher frequency, giving a higher resolution but weaker signal. 40 Hz is a very high frequency for the reservoir depth at Celo field. 15 Hz is typical of the best signal to noise ratio.

Proprietary feedback: After the initial model is run, both the processing company and client company offer feedback, the model is rerun, and more changes suggested. Changes are based off of interactive feedback from the client company.

Seismic gather: collection of seismic traces that share a common geometric attribute, imaged as 'wiggles', they represent subsurface changes in acoustic impedance.

Subsalt: Below salt.

Synthetics: Forward modeling the anticipated seismic response based on theorized impedance (from velocity and density rock properties). One-dimensional model of acoustic waves traveling vertically through the subsurface.

Trough/Peak: As the subsurface impedance (density*velocity) increases, the reflection coefficient decreases. A very dense (or fast) layer will have a high impedance that reflects more of the seismic wave. A peak represents a higher signal return (more reflection). Because the wavelets are zero-phase, the peaks or troughs are centered over the impedance changes. (Glossary figure A, sketch).

> Wavelets: A pulse from a single reflector with amplitude, frequency, and phase. (Glossary figure B, RokDoc, 2014)
>
> Zero-phase synthetic: Synthetic using zero-phase wavelets, symmetrical about time 0.

Well sidetrack: A secondary wellbore drilled at an angle to, but from within, the original hole.

## Glossary Figures

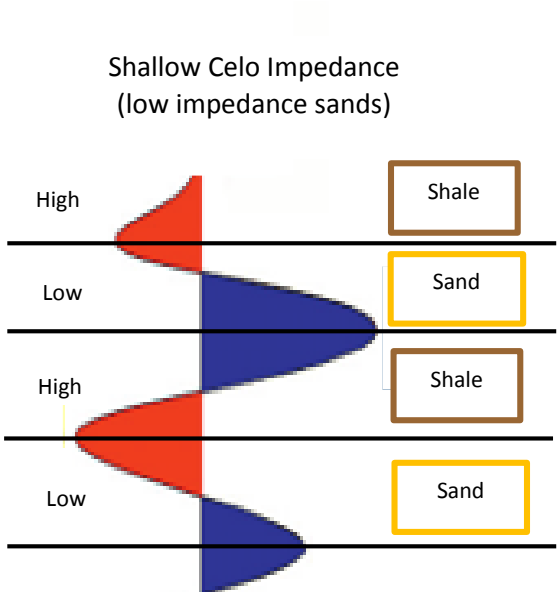


*Glossary Figure A: Sketch example of seismic wave response to changing impedances.*

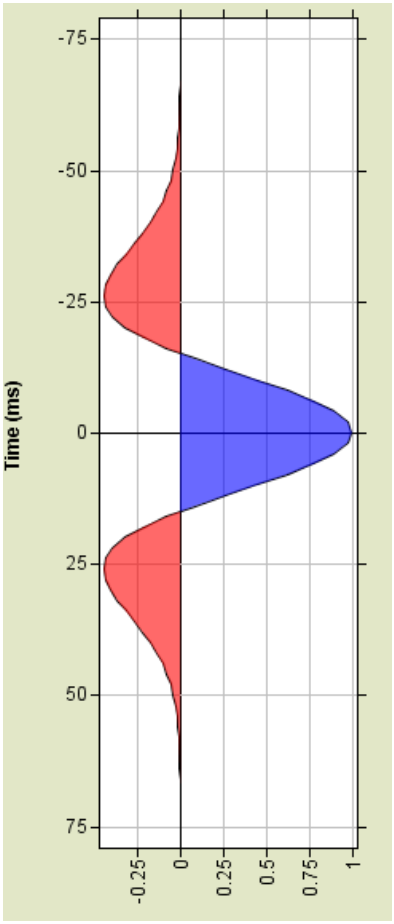


*Glossary Figure B: Zero-phase wavelet. (RokDoc, 2014).*

## Figures

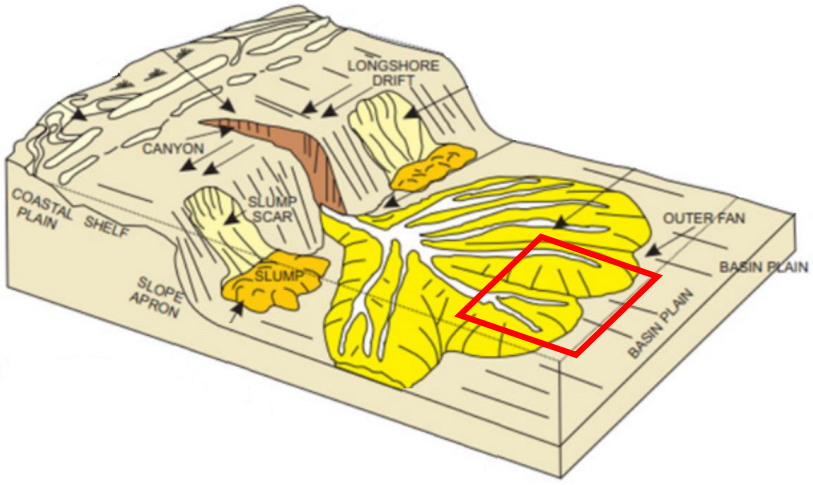


*Figure 2: Submarine fan complex, prograding. Celo field theorized environment of deposition in the red box. (Reading and Richards, 1994)*

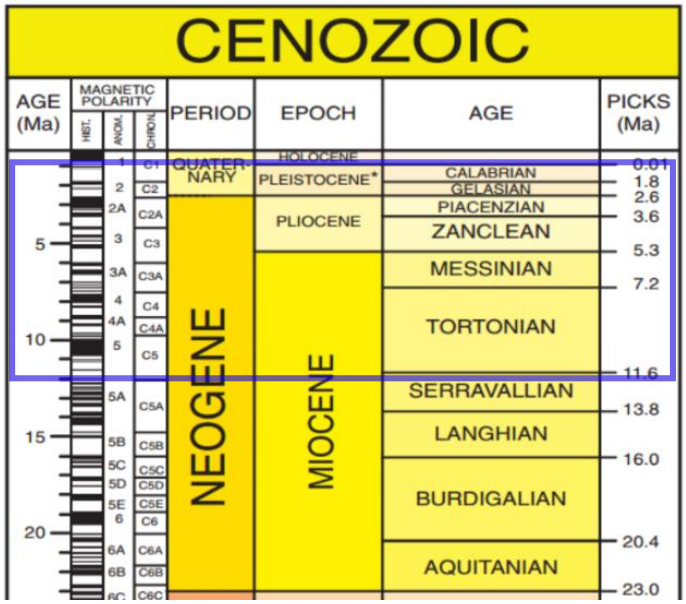


*Figure 1: Geologic time scale, blue box is the age range of the possible reservoirs in Celo field. (Walker et al. 2012).*

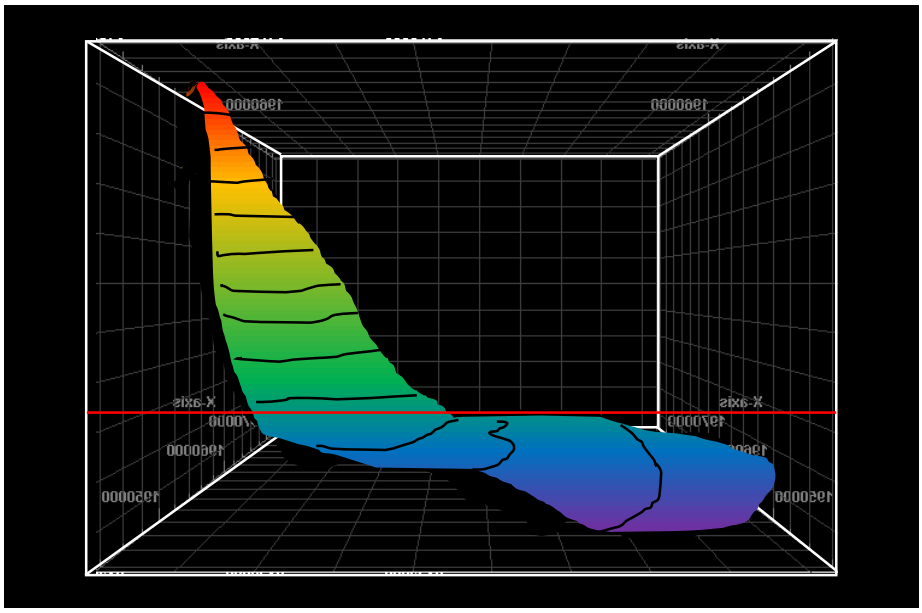

*Figure 3: 3D sketch of main reservoir structure with 5x vertical exaggeration. Contour lines and colors correspond to depth. Oil water contact in red.*

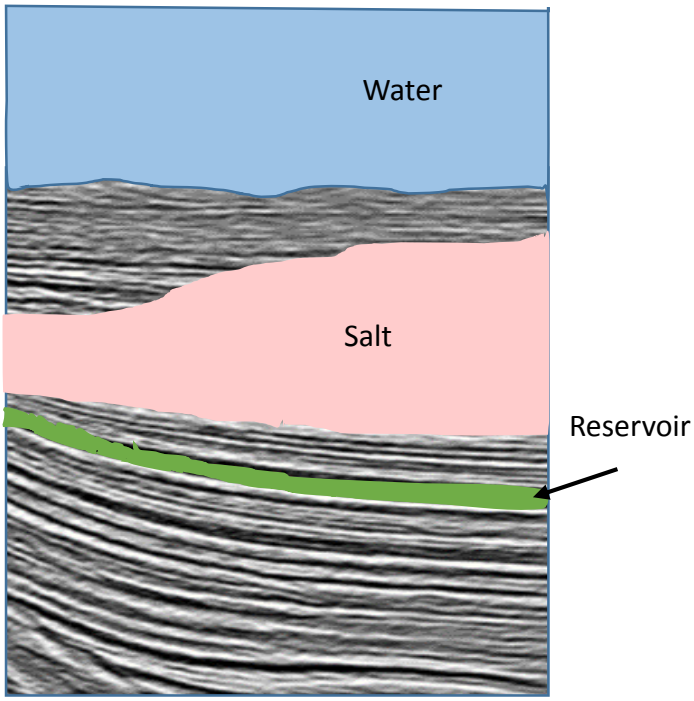


*Approximate location of reservoir relative to salt and water, side view. Seismic background from Visual Logic, 2014.*

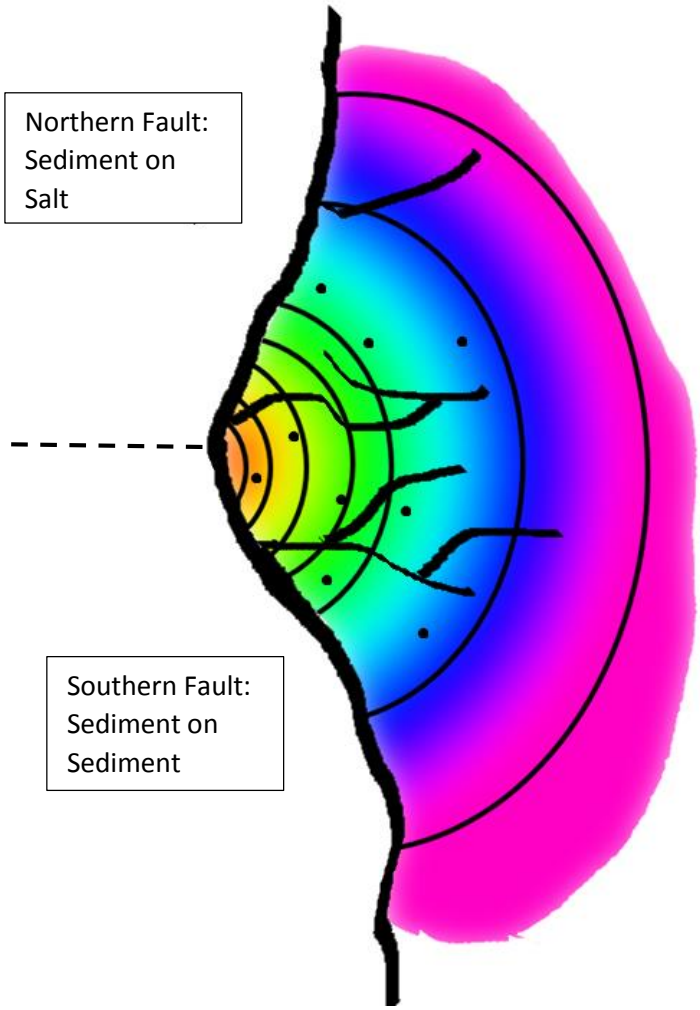


*Figure 4: Sketch of main reservoir in map view. Faults represented by black lines, wells (9) by black circles.*

G:MS Thin intermittent interval of minor sands (G: **M***inor* **S***ands*)

F:SH Shale (F: **SH***ale*)

E1:CS, E2:CS 70% NTG highly channelized sands, separated by a thin shale (E1:**C***hannel* **S***ands*, E2:**CS**)

D:CO *Debrites*, shales, highly variable cutoff (D: **C***ut* **O***ff*)

C:TB Thin beds of shale and sand with inconsistent proportions (C: **T***hin* **B***eds*)

B:MR *Main Reservoir* >95% NTG 100' blocky massive sands punctuated with 10' marls, high porosity (B: **M***ain* **R***es*)

A:LC Sands with volcanics, clastics, extensive lateral compartmentalization (A: **L***ateral* **C***ompartmentalization*) (not shown on log)

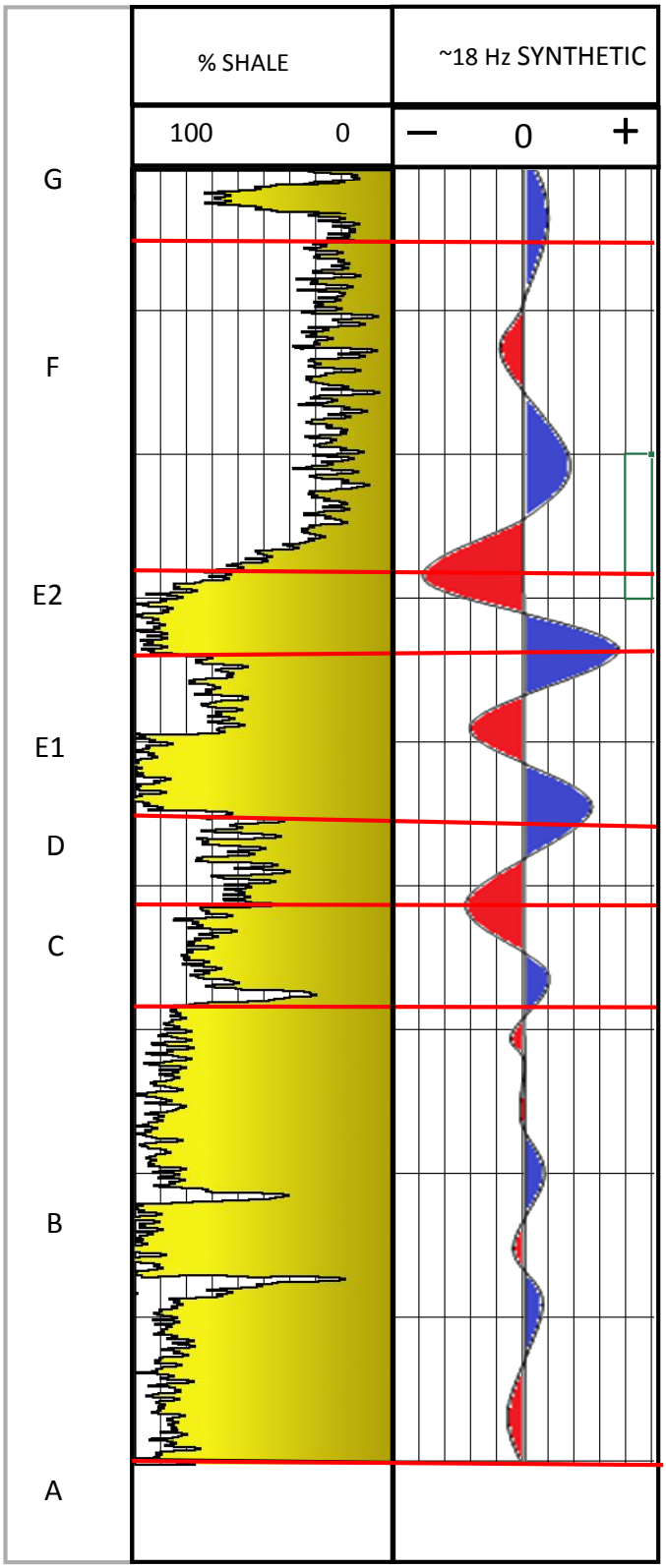


*Figure 5: Sketch example of a typical Celo field well log with % shale and synthetic response.*

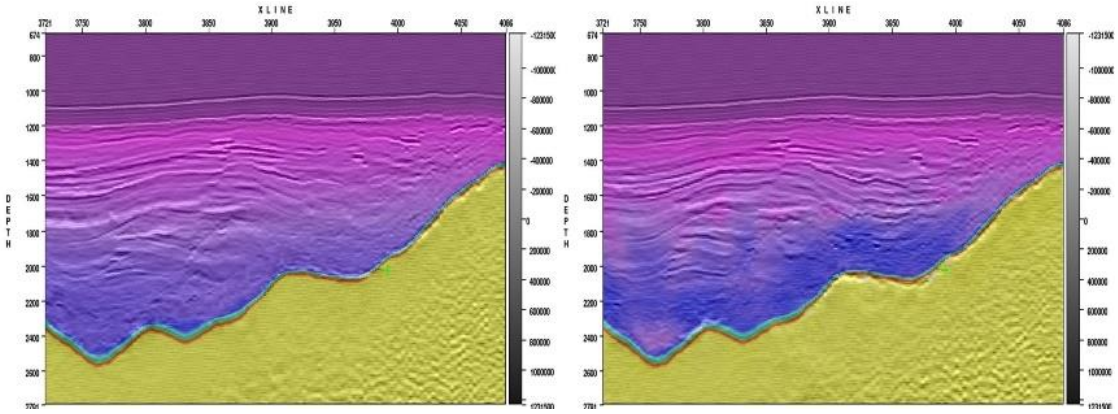


*Figure 6: Before and after FWI application. Color represents the relative velocities of the velocity model with the shaded seismic in the background, Chao et al. 2014.*

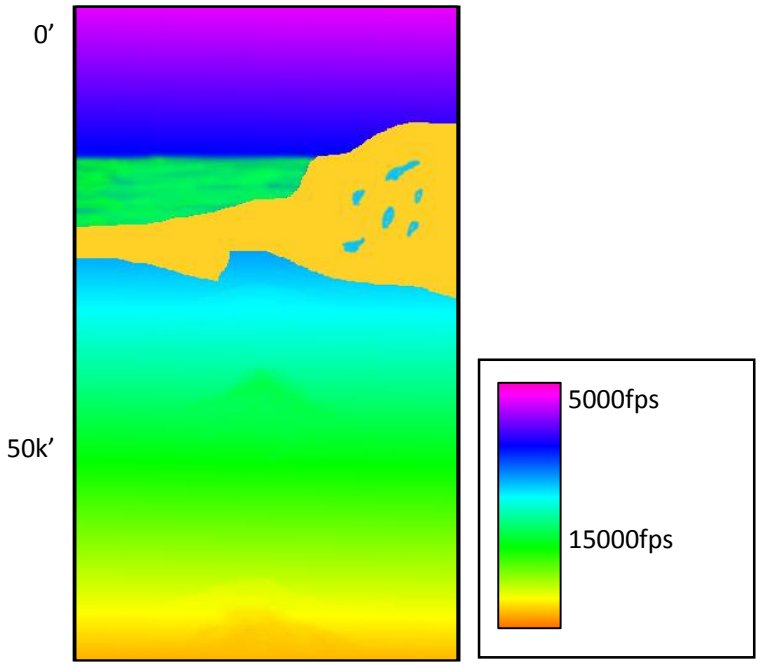


*Figure 7: Sketch of VM1 velocity model with scale.*

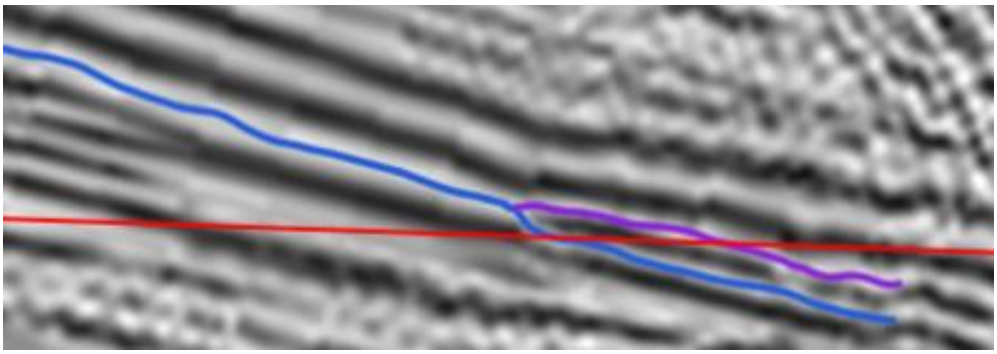

*Figure 8: Example of the reflector fork at the top of interval B. OWC in red. Background seismic from Huuse, 2008.*

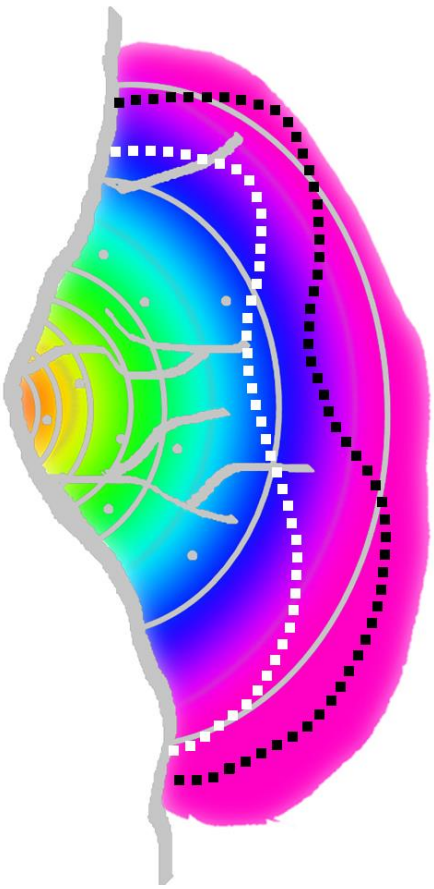

*Figure 9: Sketch map view of the top of interval B. White dashed line is the lowfork OWC, black dotted line is highfork OWC.*

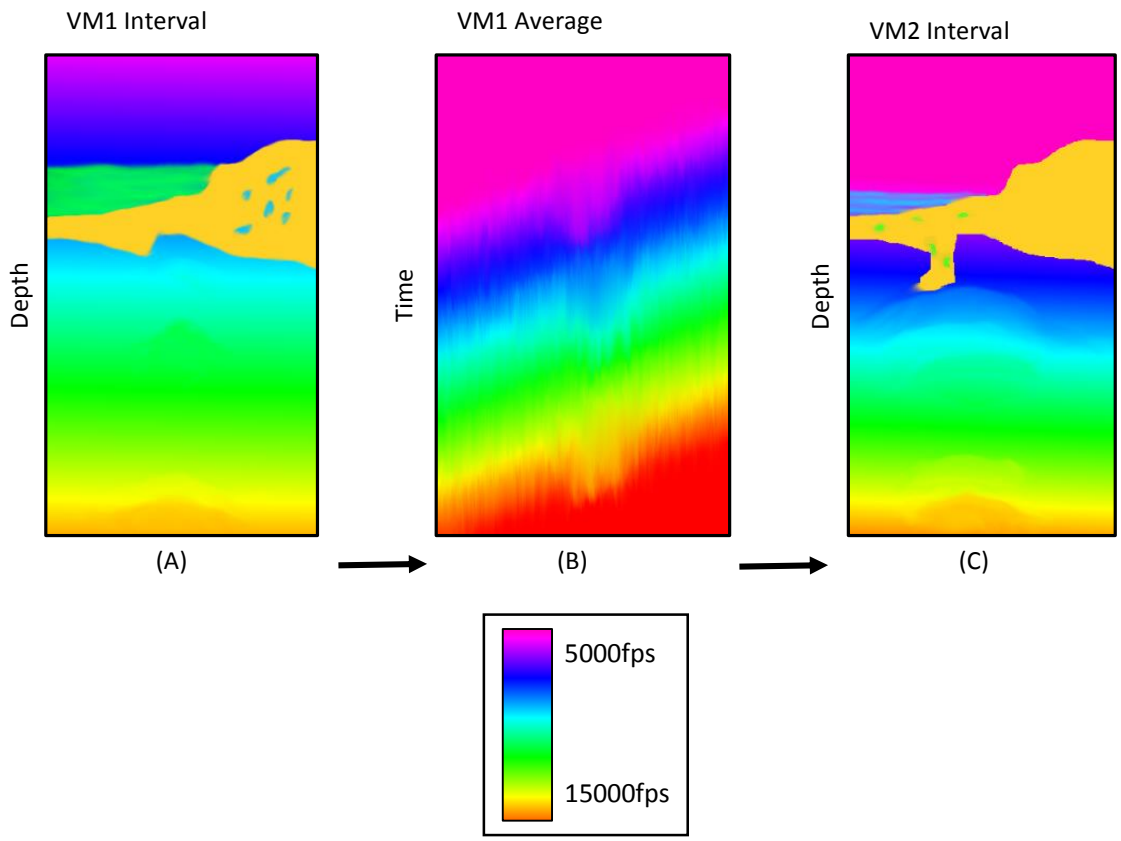


*Figure 10: Sketches of (A) VM1 Interval, (B) VM1 Average, and (C) VM2 Interval velocity models.*

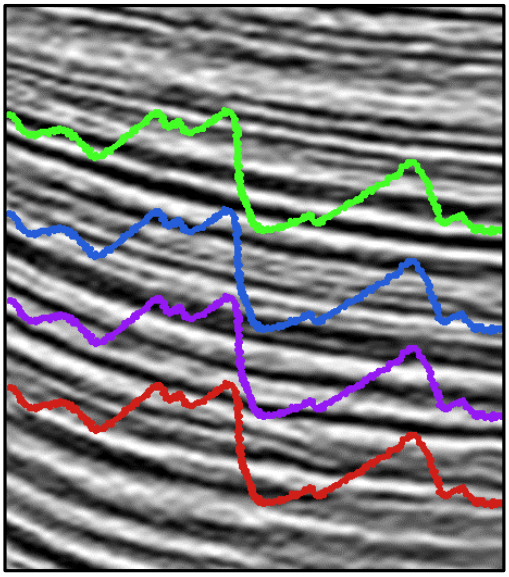

*Figure 11: Sketch of 'jitters' as seen after depth converting horizons through various velocity models.*

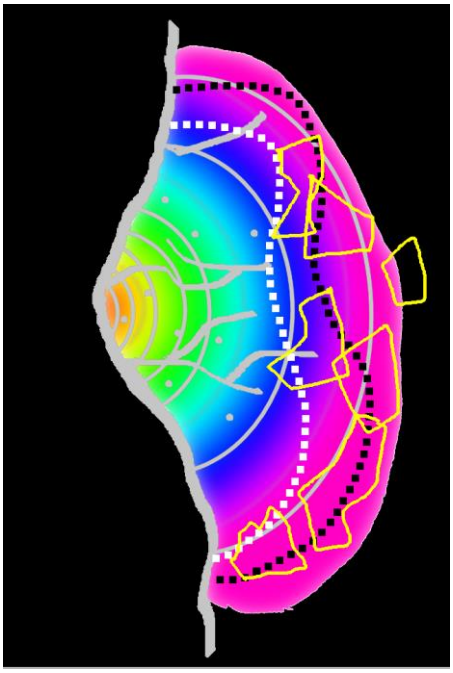

*Figure 12: Sketch of polygons of uncertainty (yellow) on map view of interval B:MR with low and high fork OWCs.*

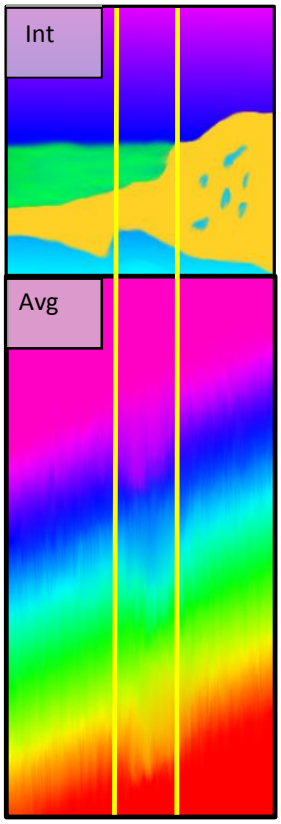


*Figure 13: Sketch of striping (bracketed by yellow) on interval and average velocity models.*

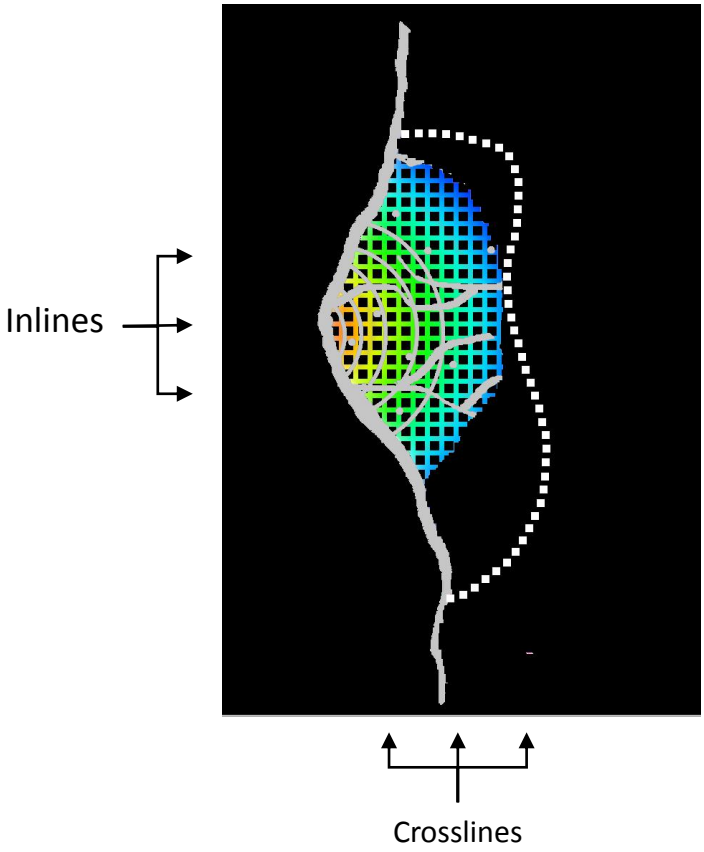


*Figure 14: Sketch of the core team interpretation up-structure of the flank fork.*

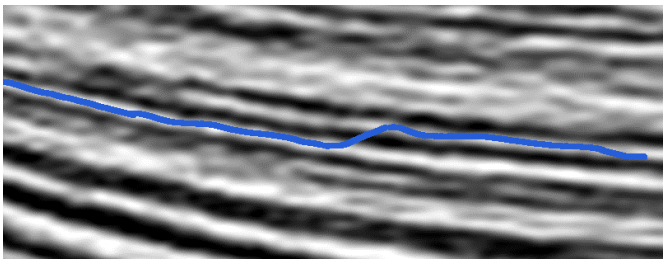

*Figure 15: Sketch example of an interpretation crossing reflectors.*

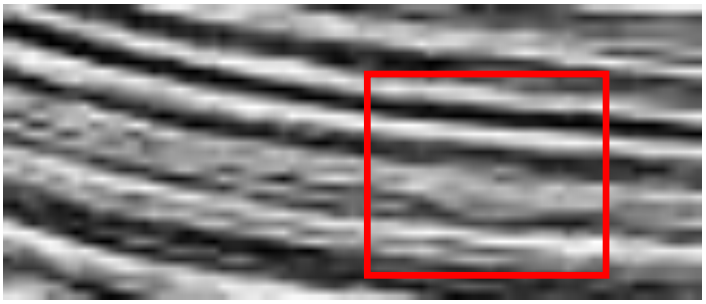

*Figure 16: Example of a possible channel in seismic data (red box). Background seismic from Huuse, 2008.*

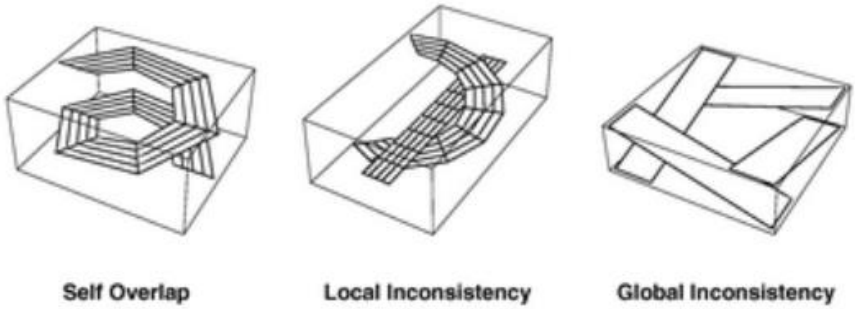


(A) (B) (C)

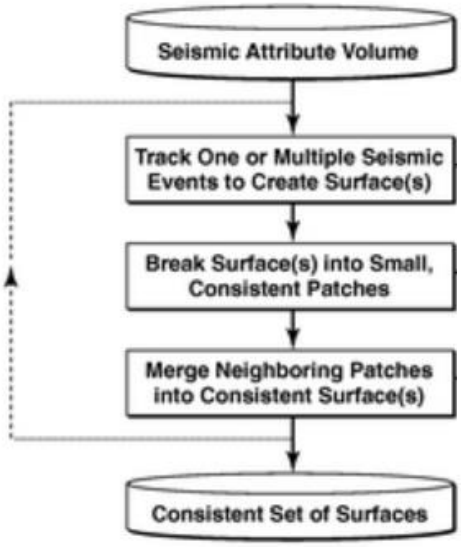


(D)

*Figure 17: Conditions for surface rejection (A, B, C). Skeletonization steps (D). Matthias, 2011.*

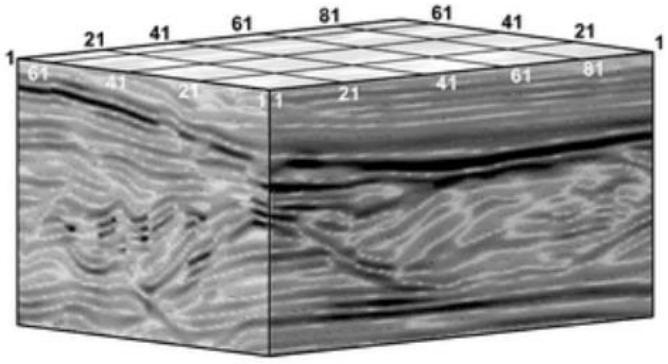


(A)

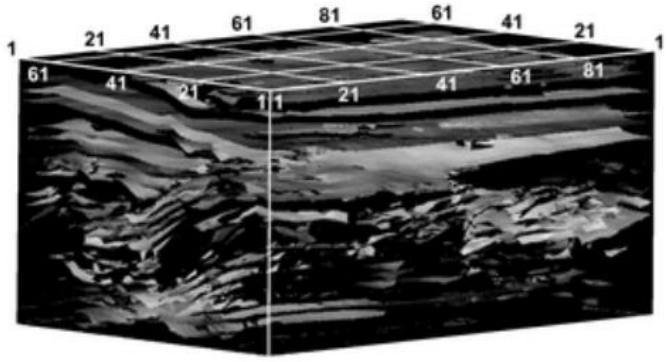


(B)

*Figure 18: Example of seismic data before (A) and after (B) skeletonization. Matthias, 2011.*

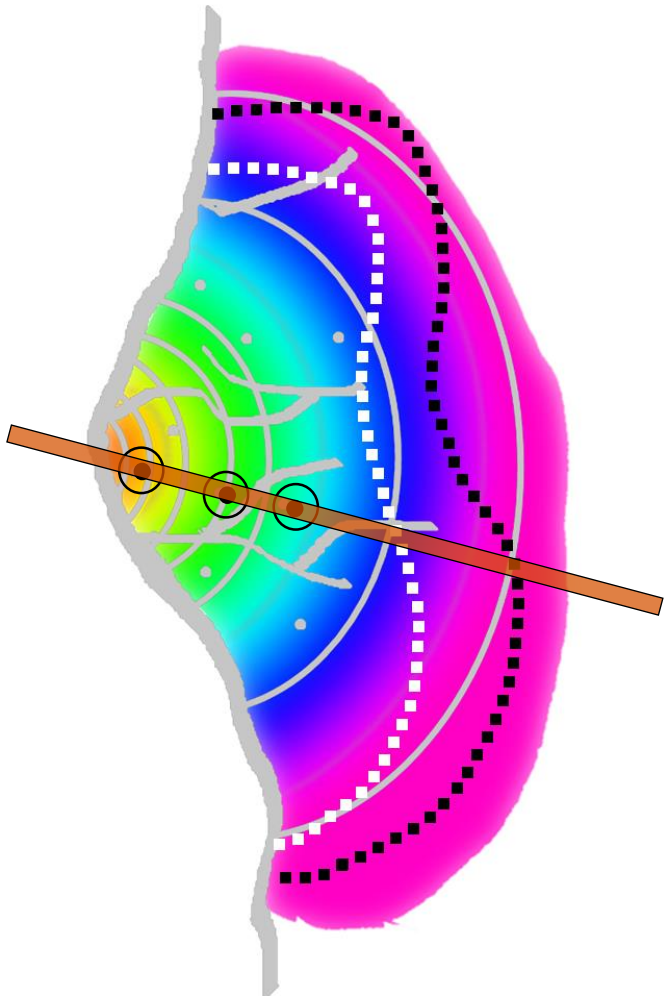

*Figure 19: Sketch, B:MR in map view with selected inline and wells highlighted.*

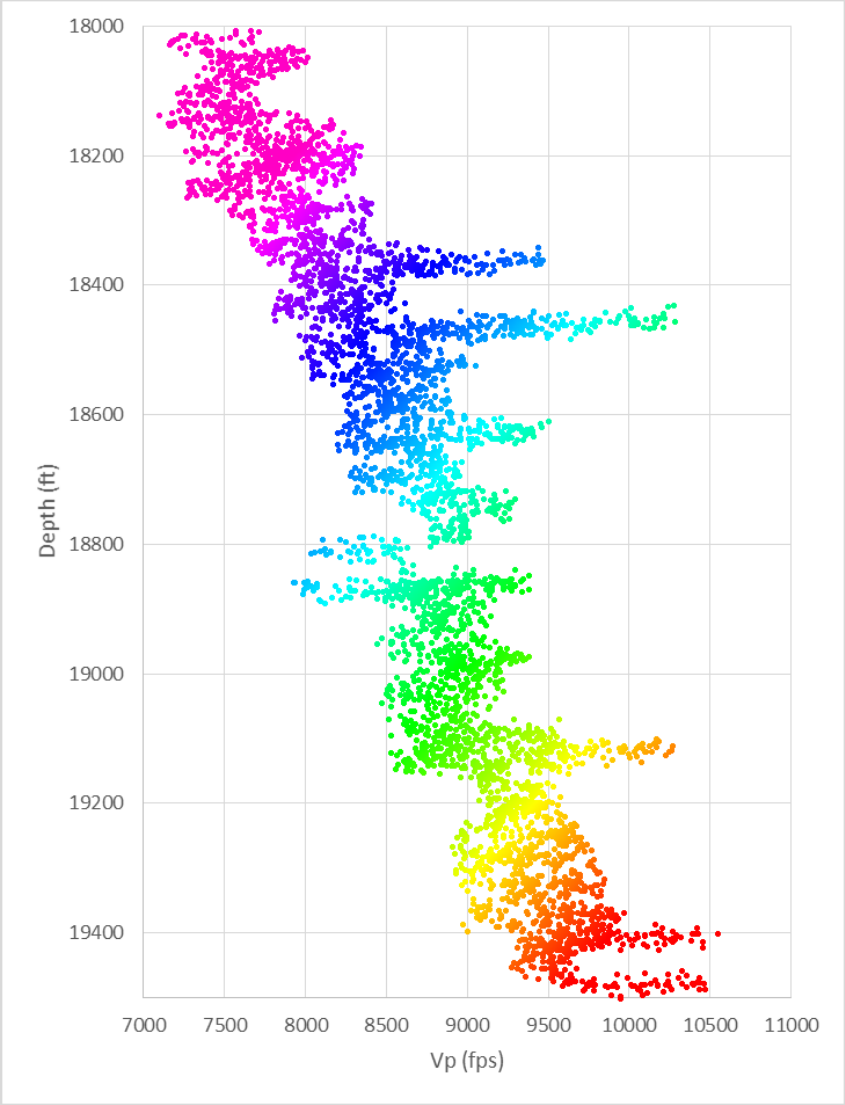


*Figure 20: Example crossplot showing velocity changes with depth for B:MR interval. Color corresponds to impedance.*

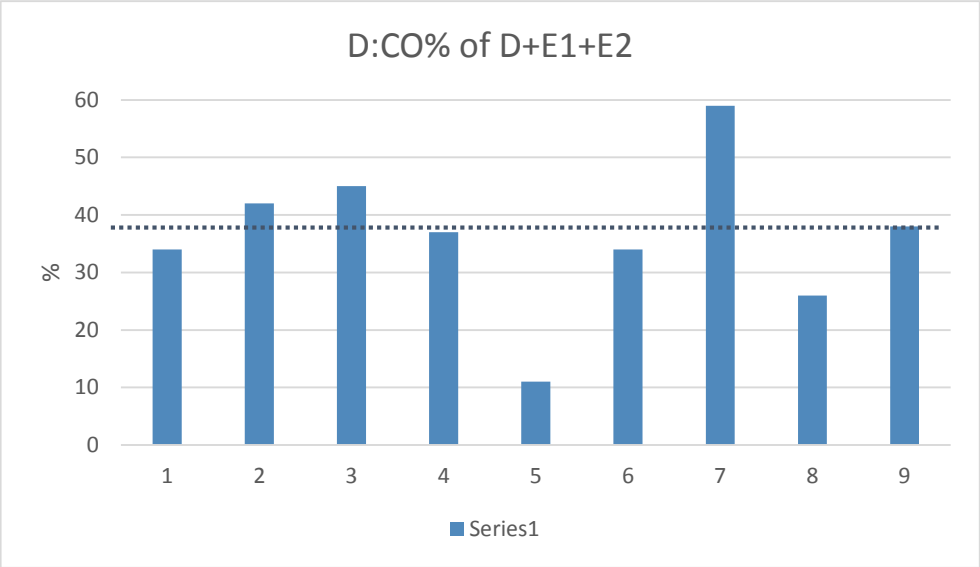


*Figure 21: Graph of unit D:CO thickness as a percentage of D:CO+E1:CS+E2:CS. The dotted line is the average, 35%.*

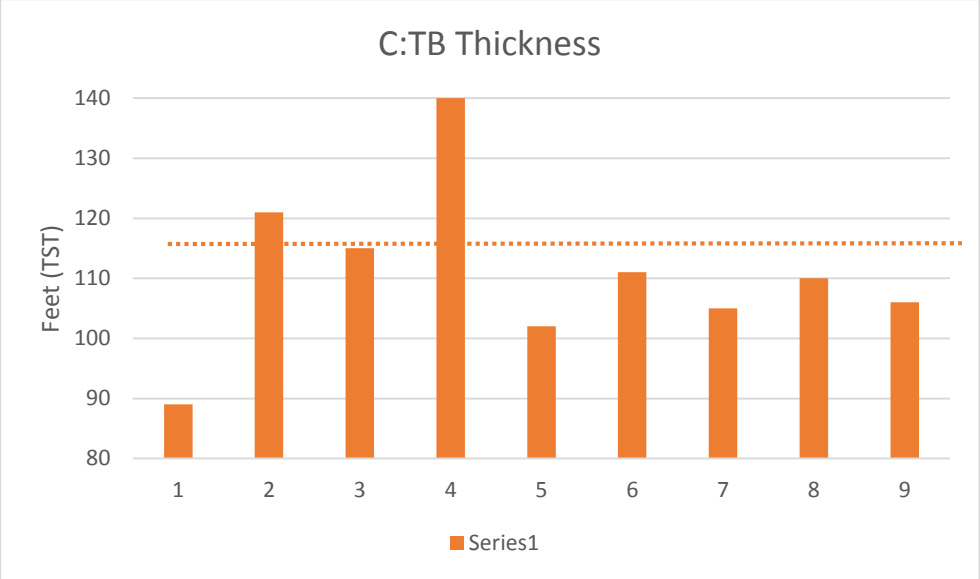


*Figure 22: Graph of unit C:TB thickness. The dotted line is the average, 110'.*

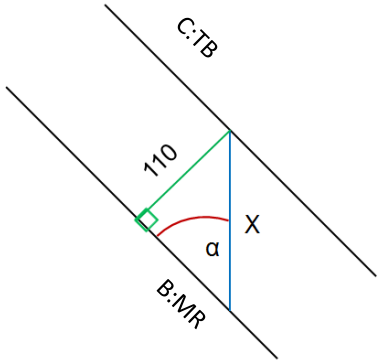


*α =Dip angle*

*X=B:MR-(110/sin(90-B:MR / Dip angle)*

*Figure 23: Method for calculating thickness of C:TB while preserving TST using dip angle.*

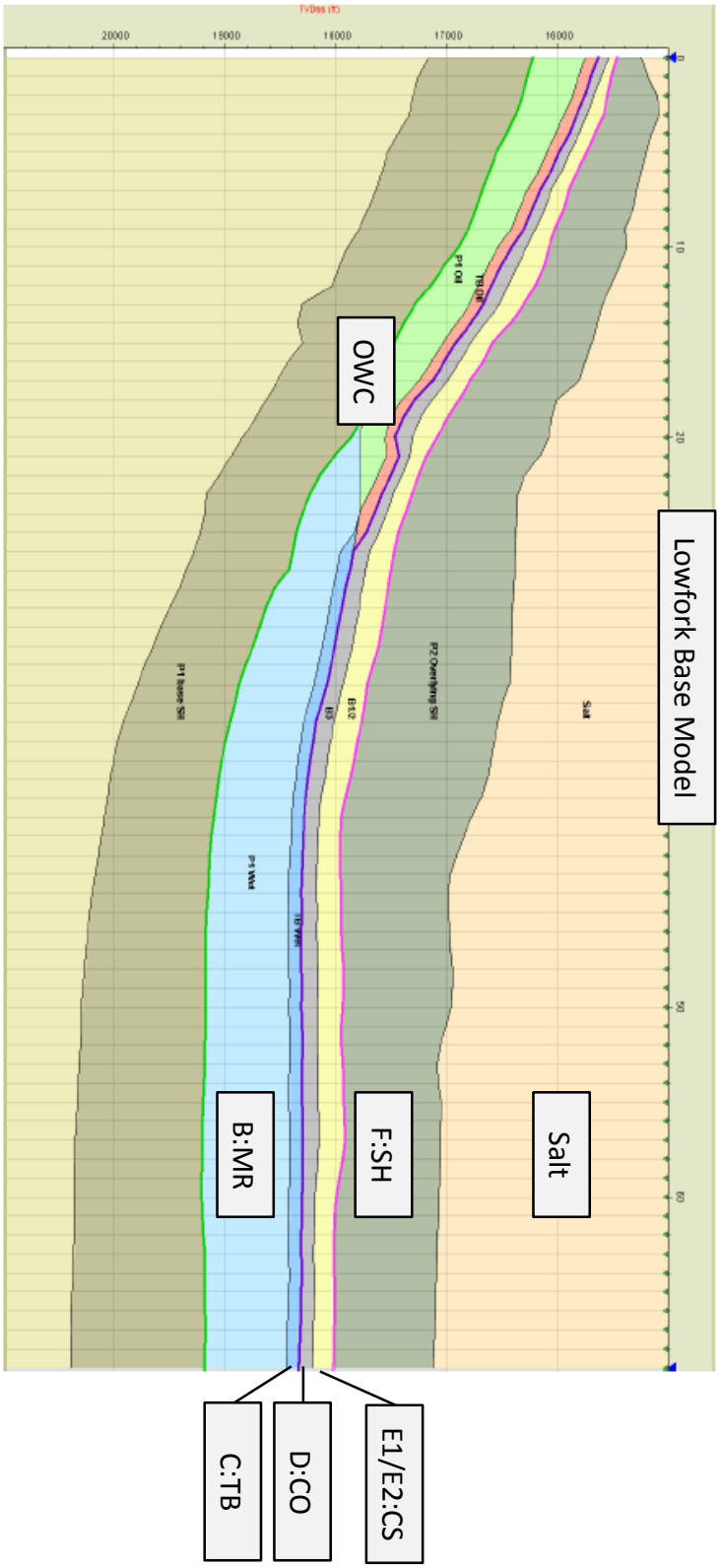


*Figure 24: Lowfork base model*

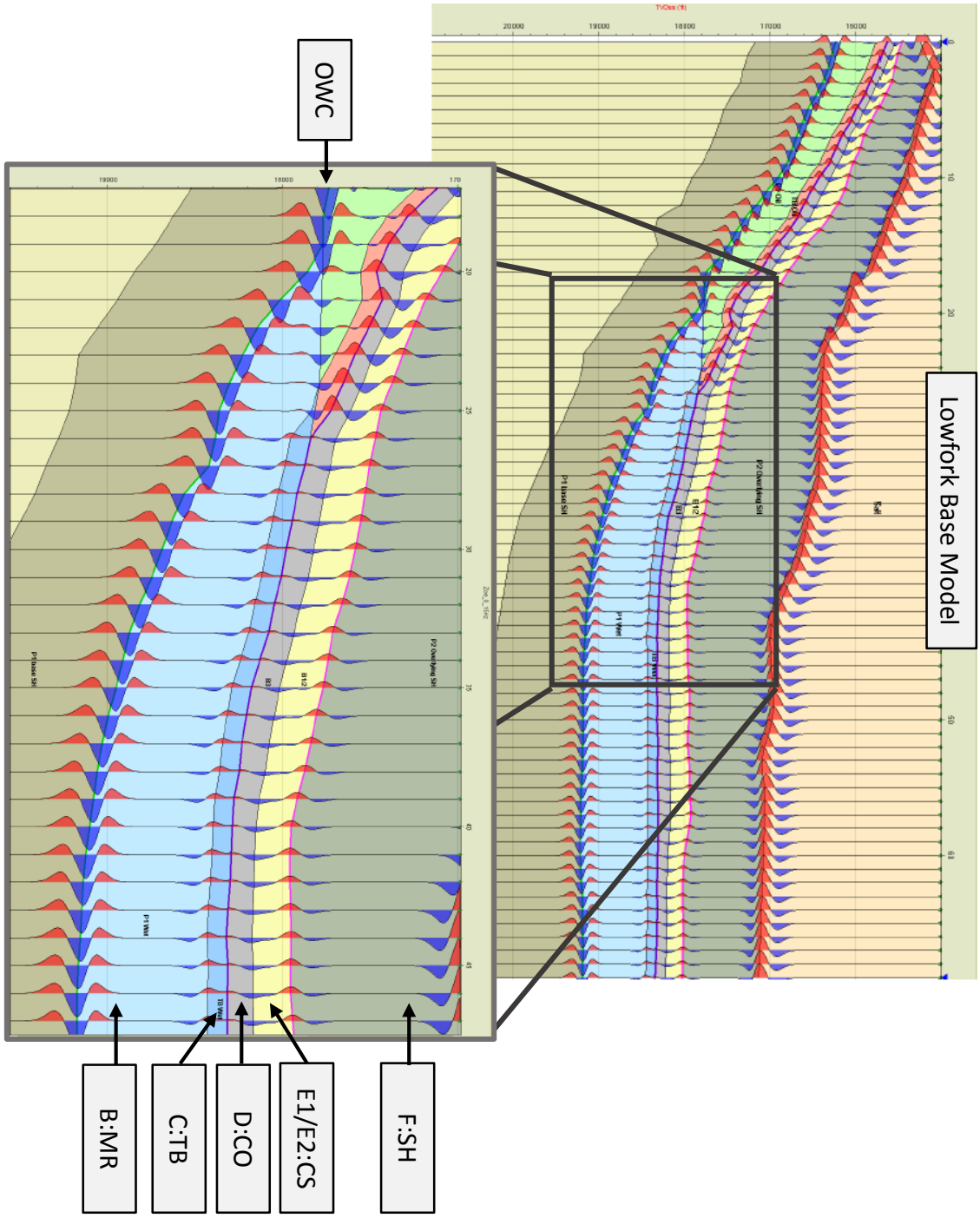


*Figure 25: Base Lowfork model with synthetics, full view and zoomed.*

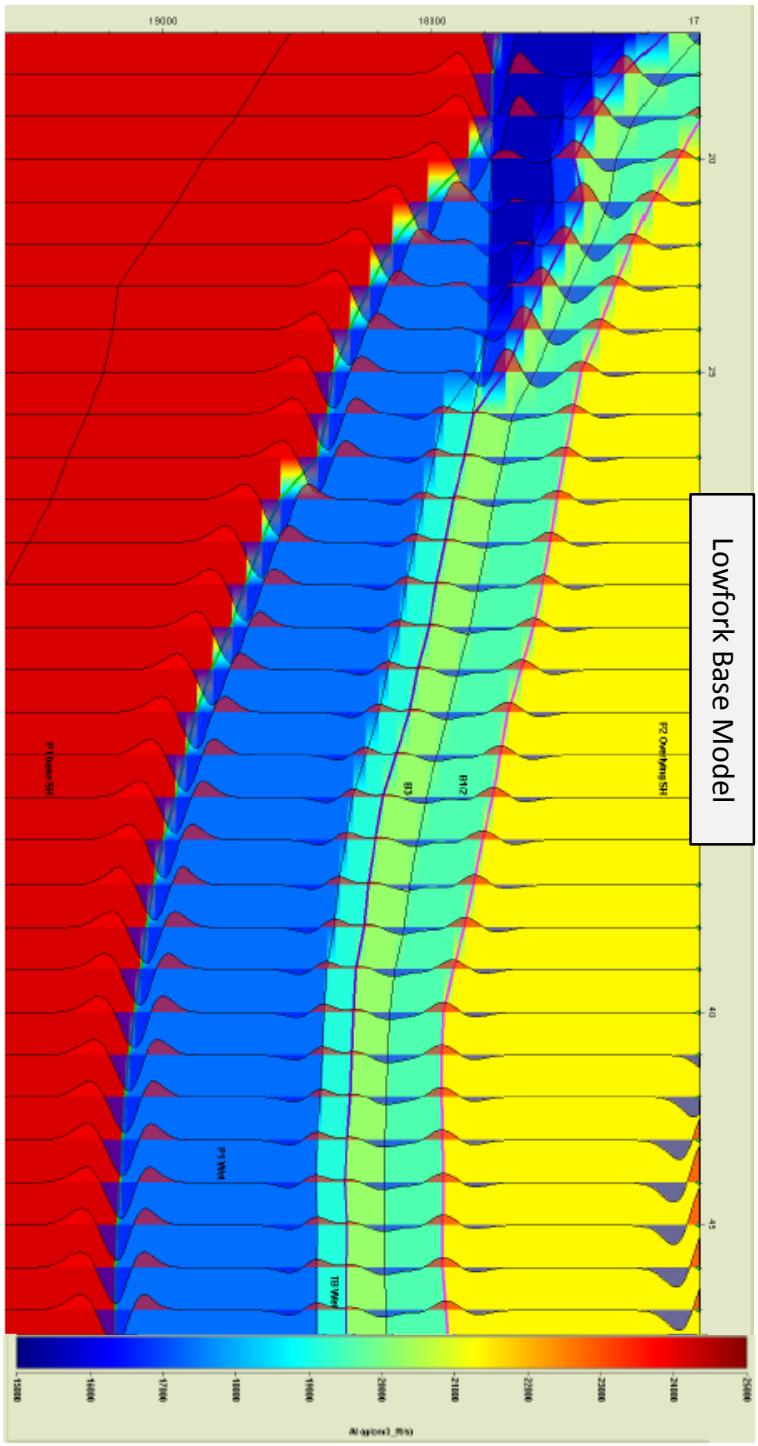


*Figure 26: Relative impedances of Lowfork Base model, zoomed.*

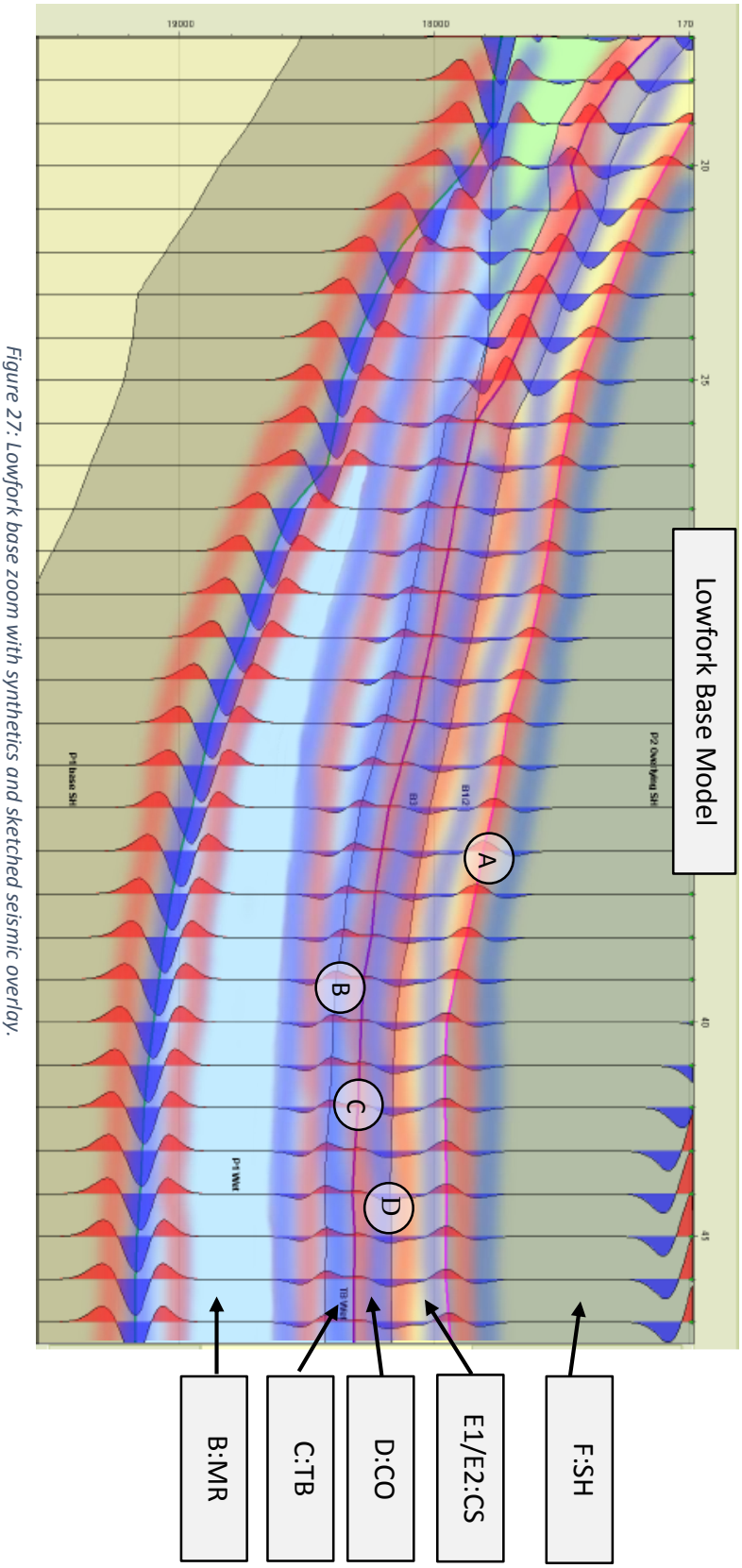


*Figure 27: Lowfork base zoom with synthetics and sketched seismic overlay.*

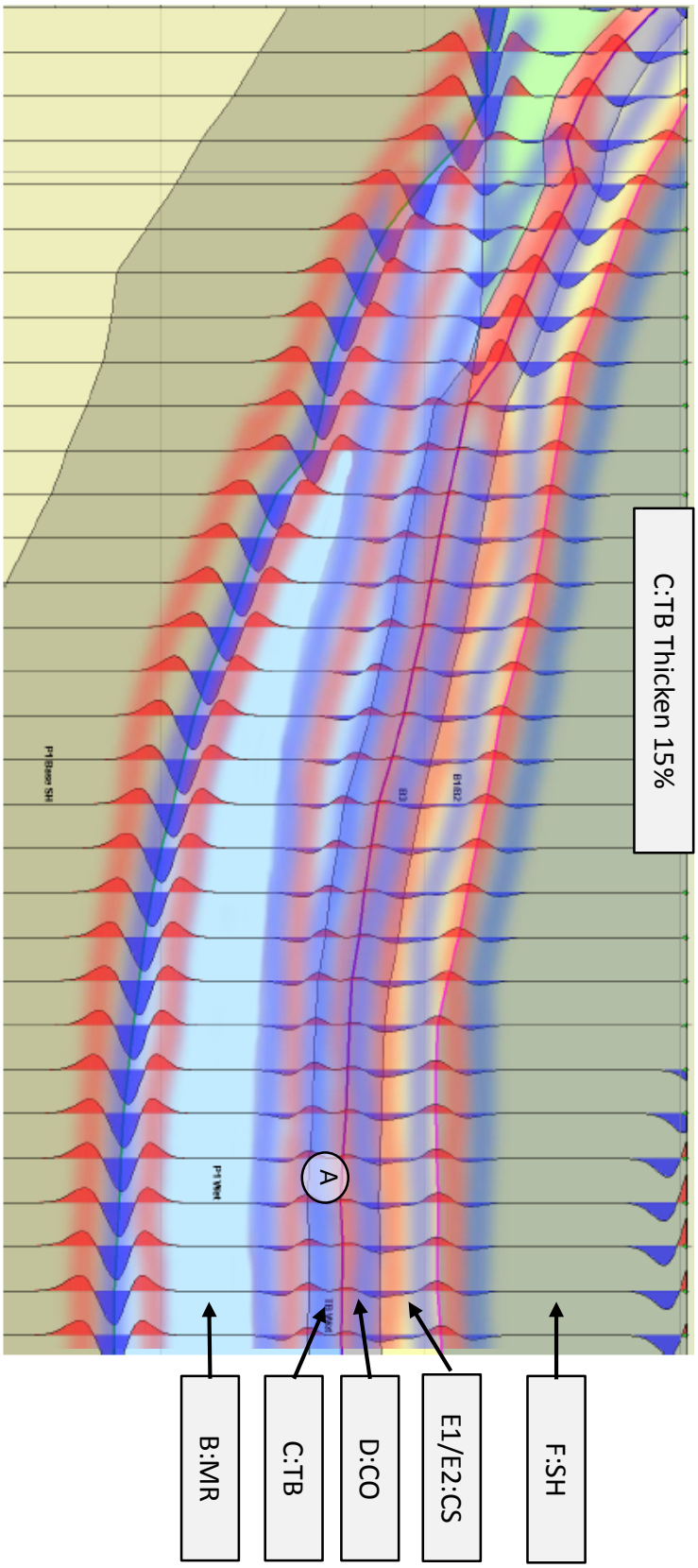


*Figure 28: Zoom view of thickening C:TB 15% with synthetics and sketched seismic overlay.*

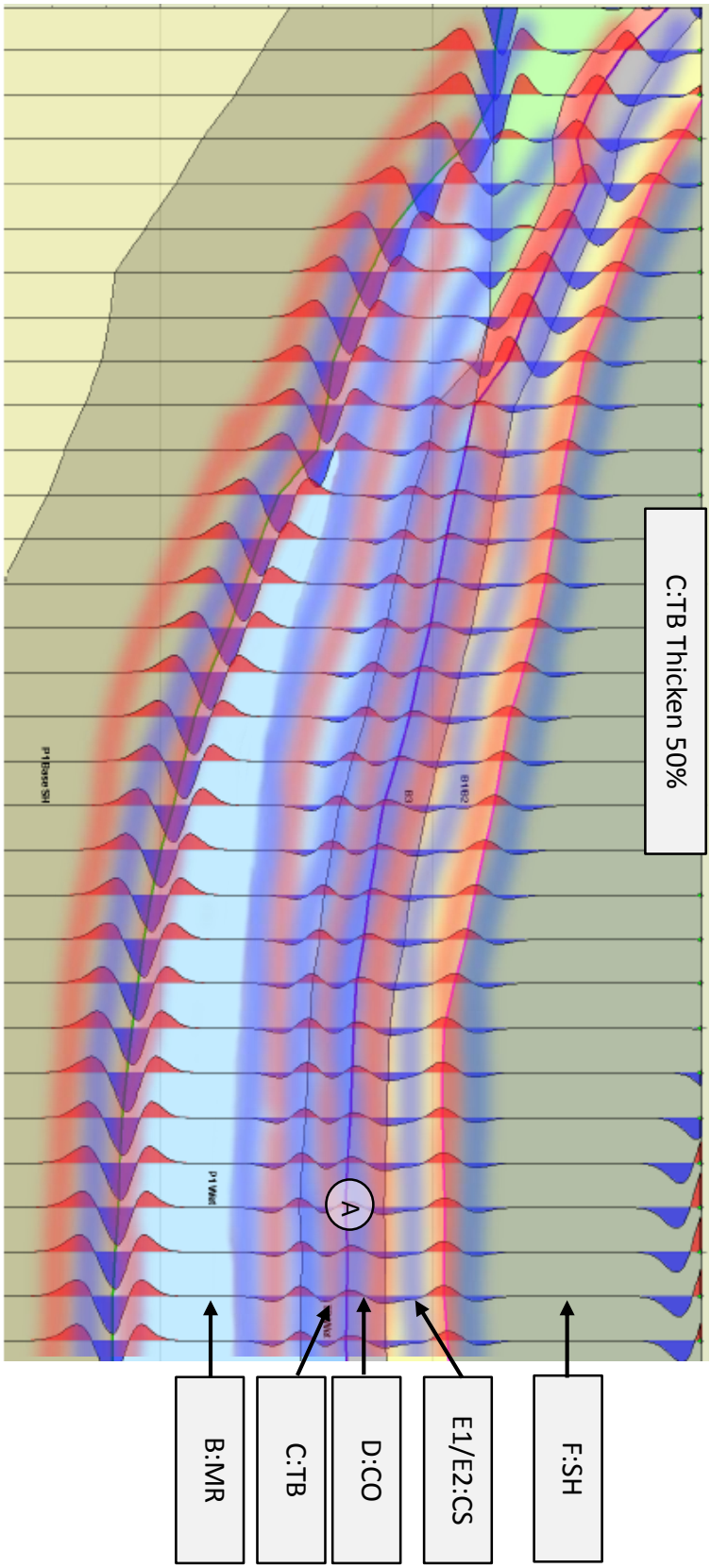


*Figure 29: Zoom view of thickening C:TB 50% with synthetics and sketched seismic overlay.*

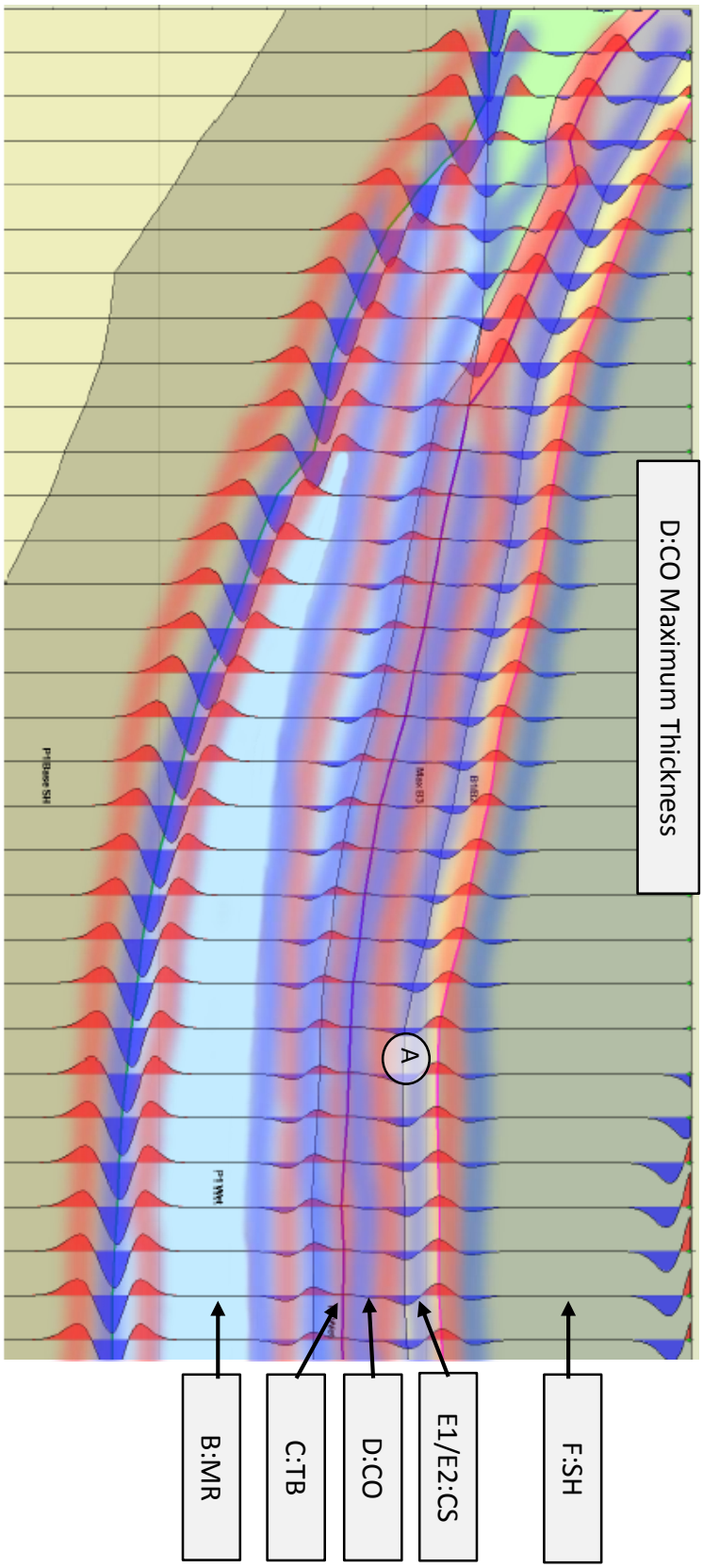


*Figure 30: Zoom view of maximum thickness D:CO with synthetics and sketched seismic overlay.*

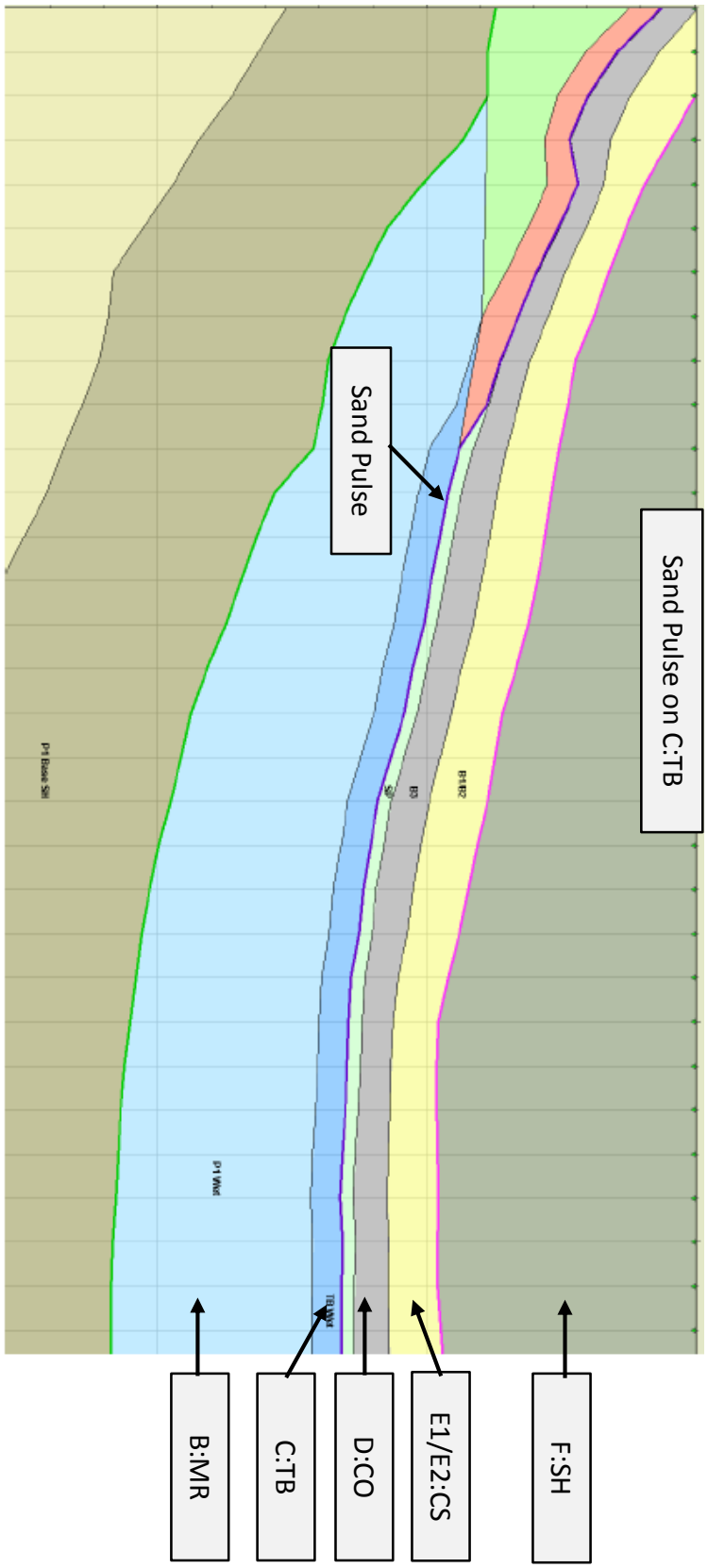


*Figure 31: Zoom view of sand pulse on top of C:TB.*

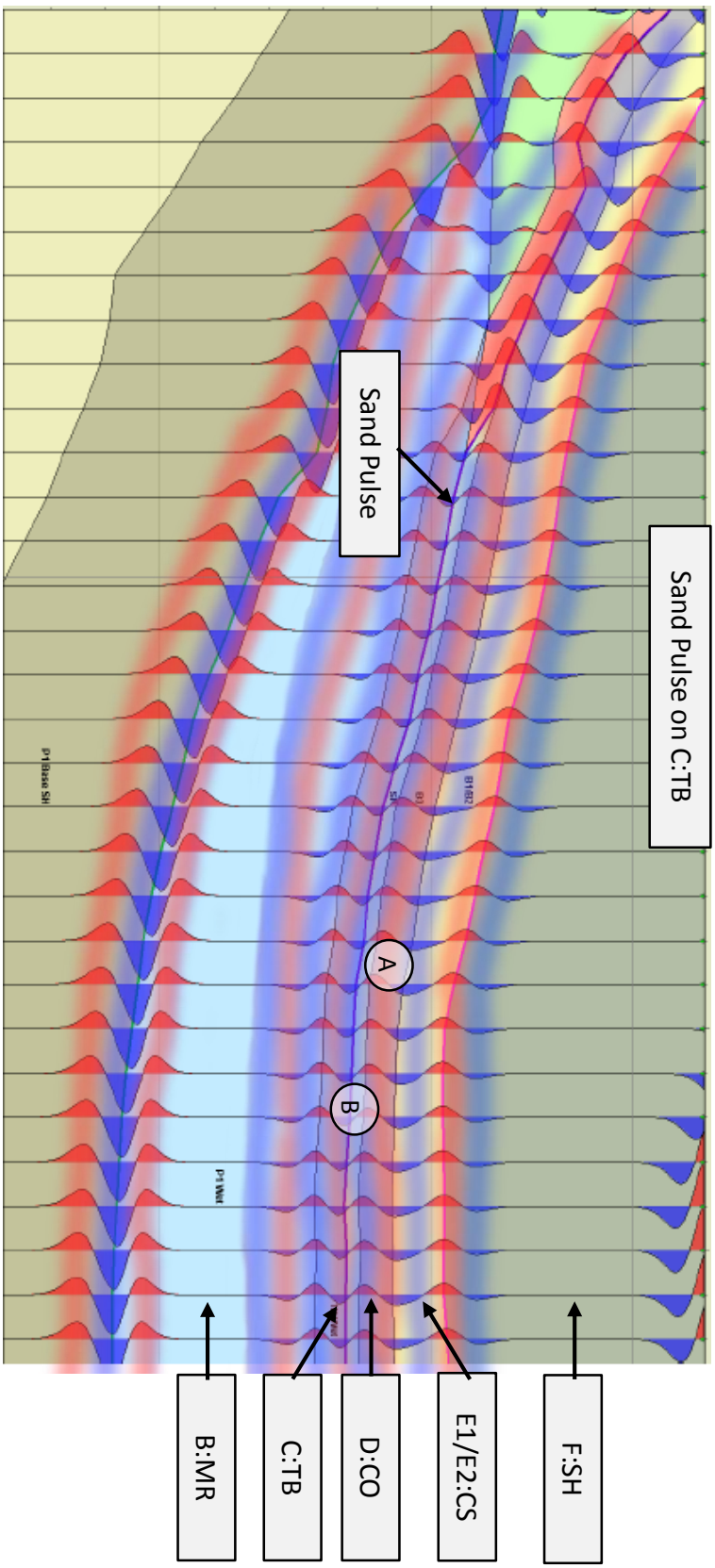


*Figure 32: Zoom view of Sand Pulse on C:TB with synthetics and sketch seismic overlay.*

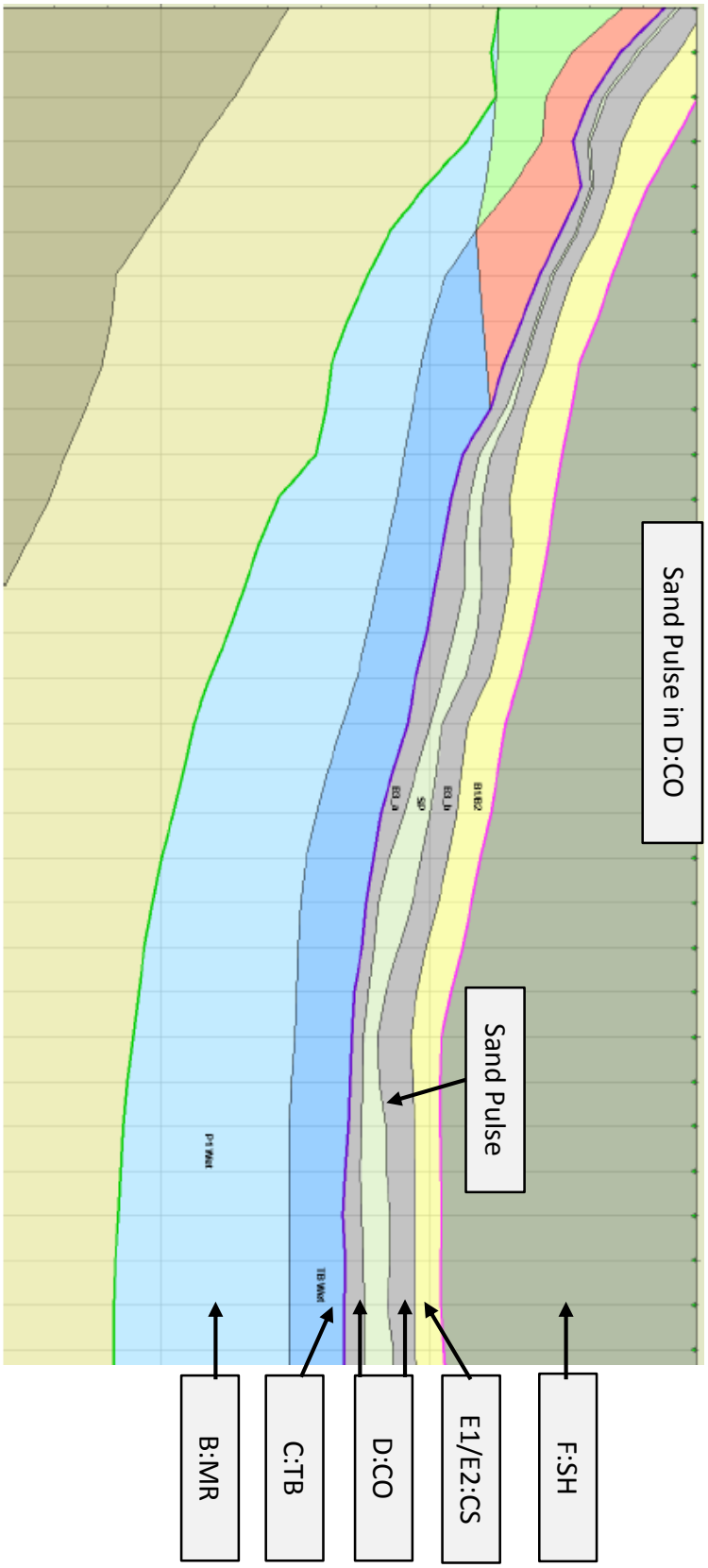


*Figure 33: Zoom view of sand pulse within D:CO*

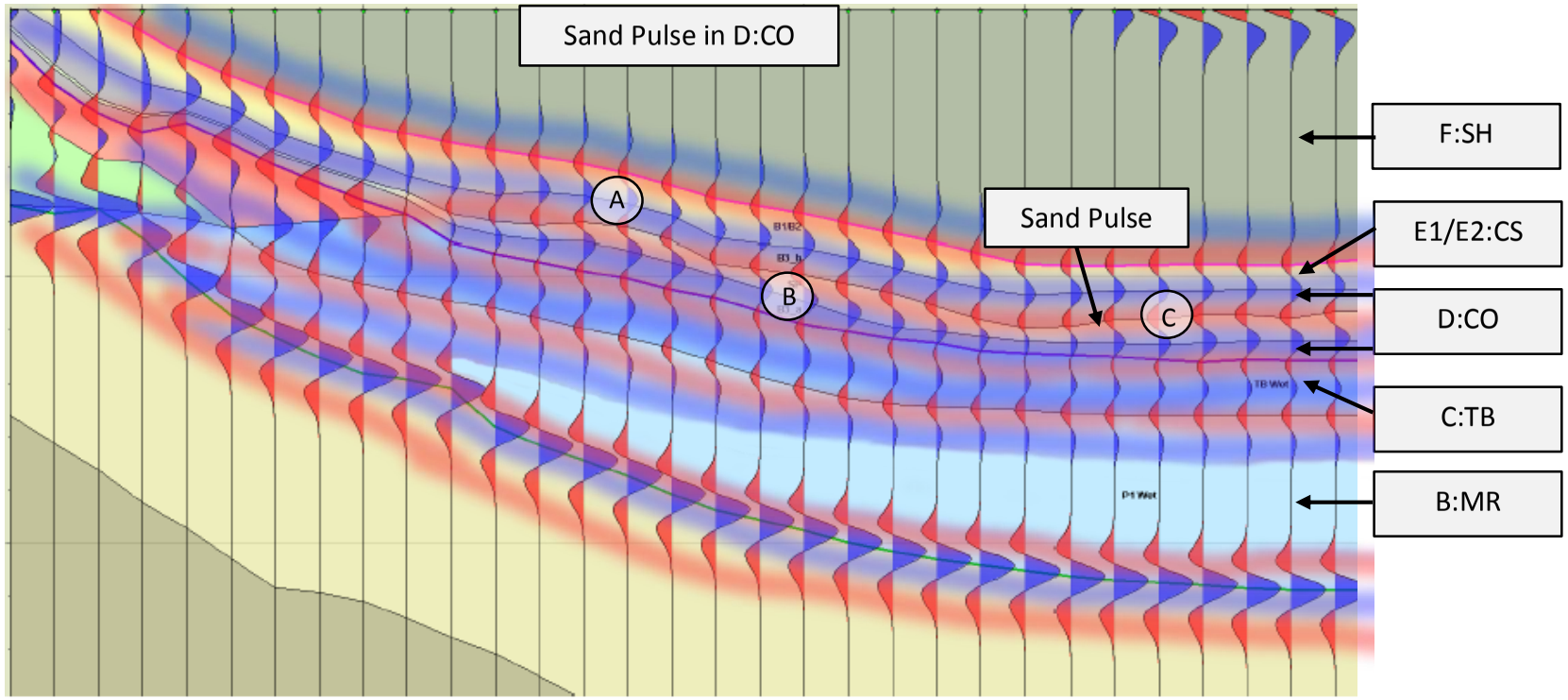


*Figure 34: Zoom view of sand pulse within D:CO with synthetics and sketch seismic overlay.*

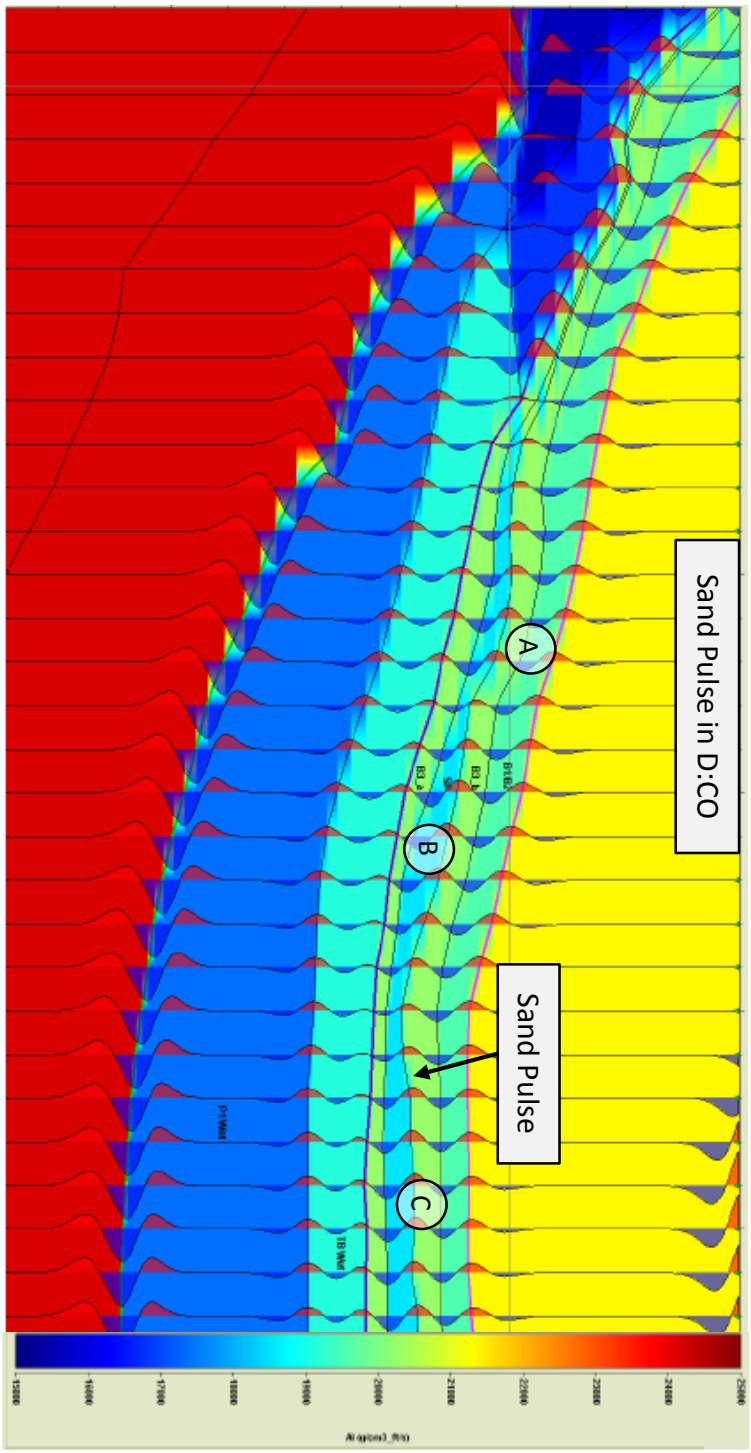


*Figure 35: Zoom view of sand pulse within D:CO, relative impedances.*

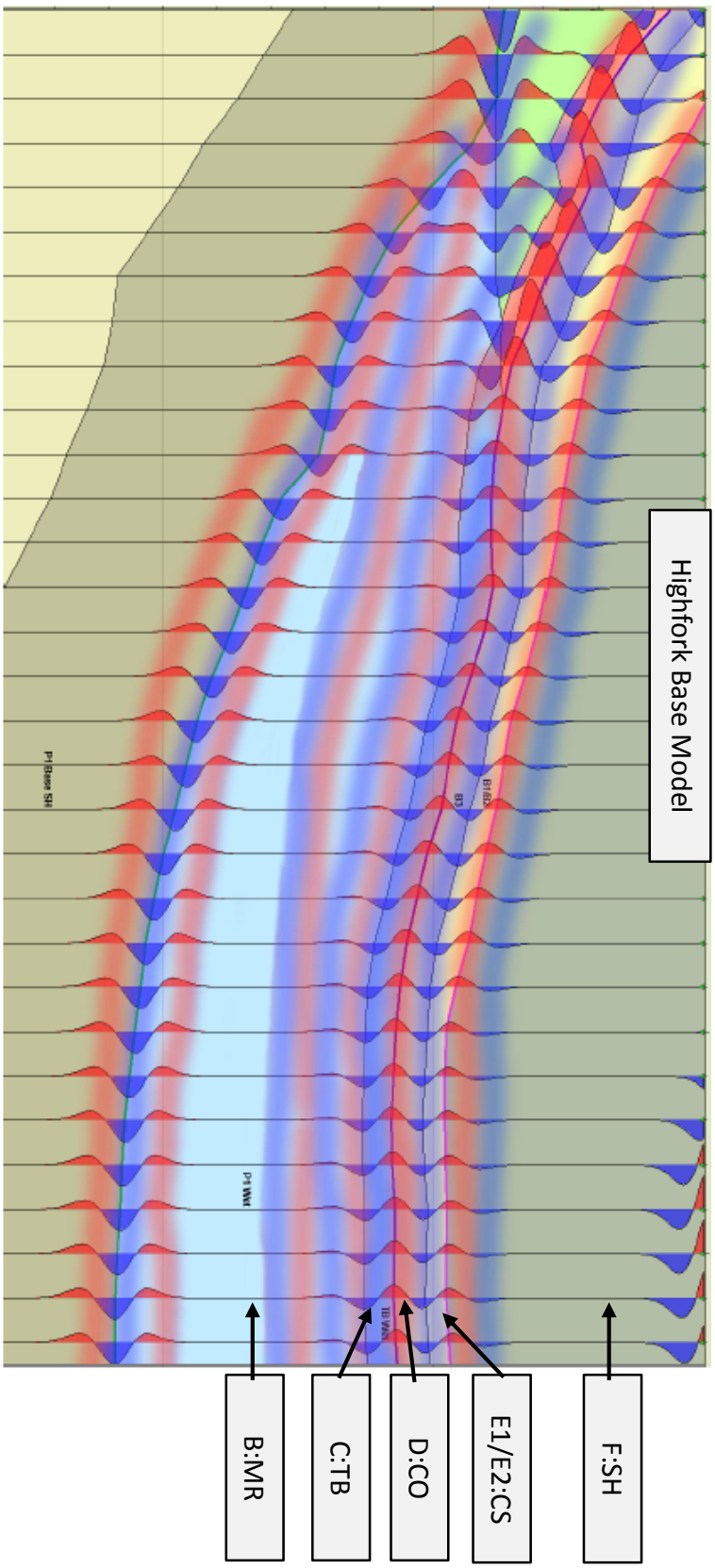


*Figure 36: Zoom view of High Fork base model with synthetics and sketch seismic overlay.*

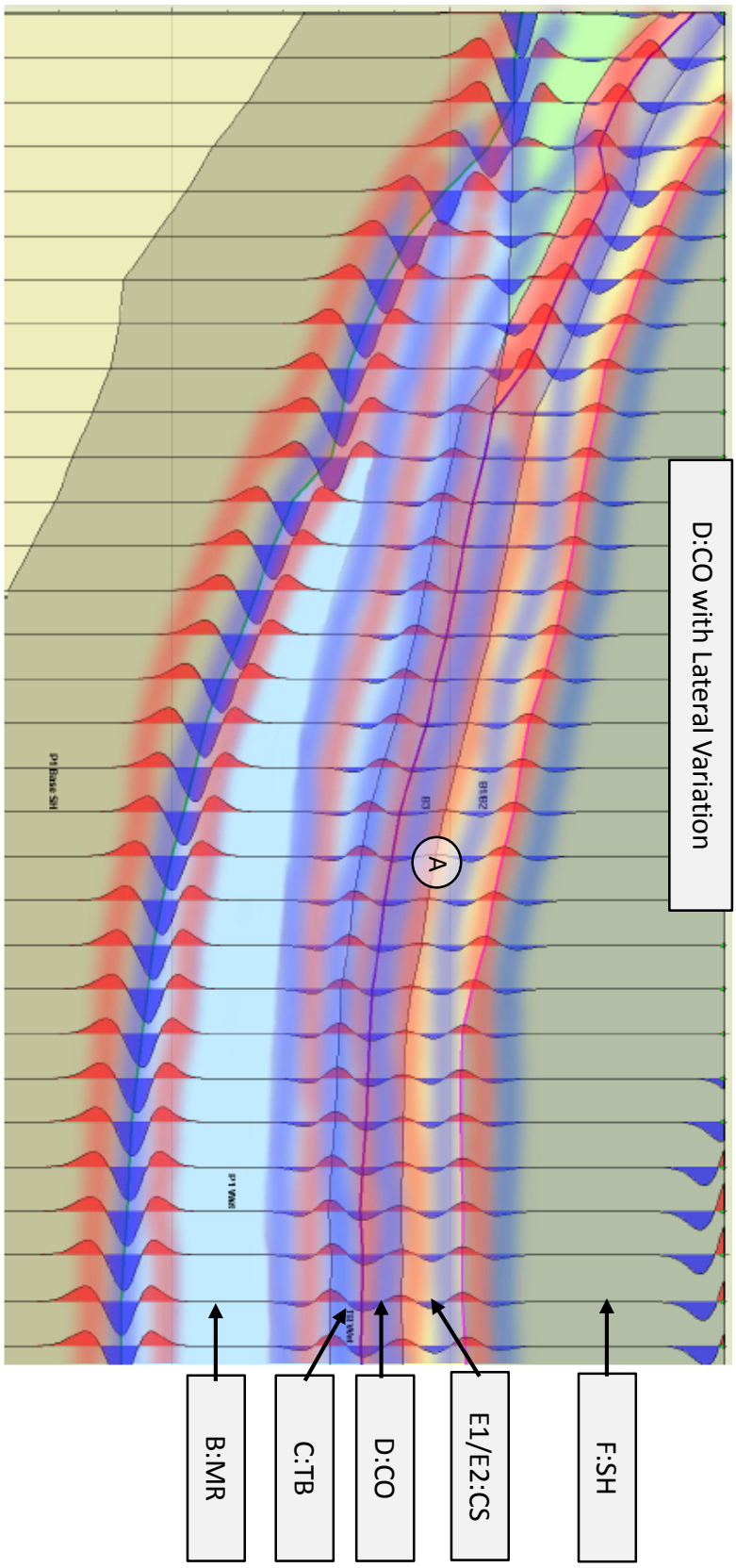


*Figure 37: Zoom view of D:CO lateral changes model with synthetics and sketch seismic overlay.*

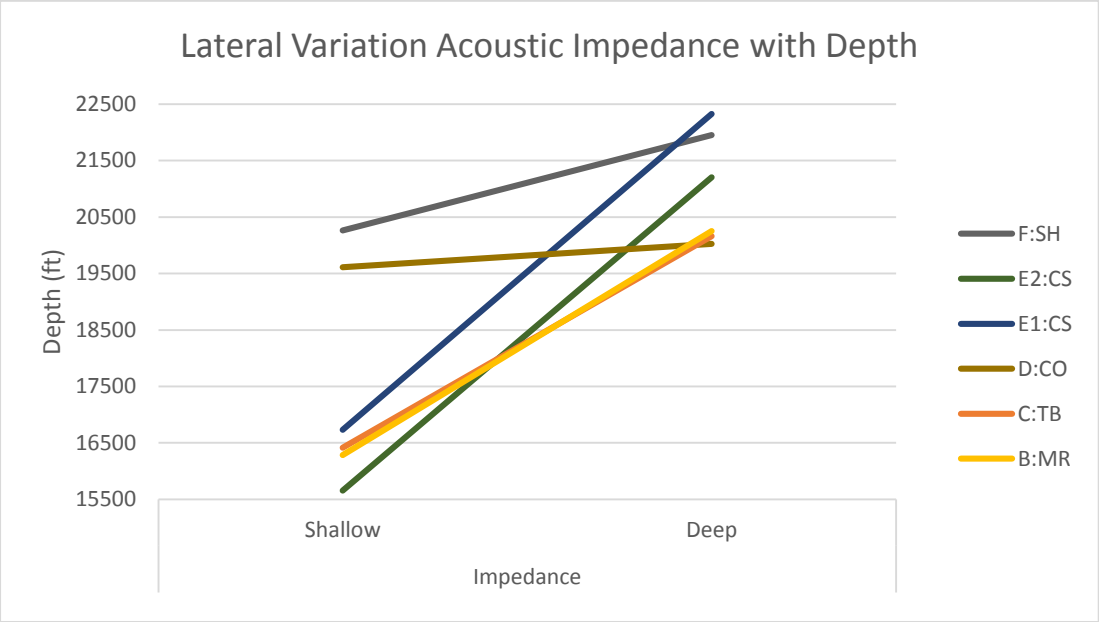


*Figure 38: Graph of the change in AI with depth for Lateral Variation Model.*

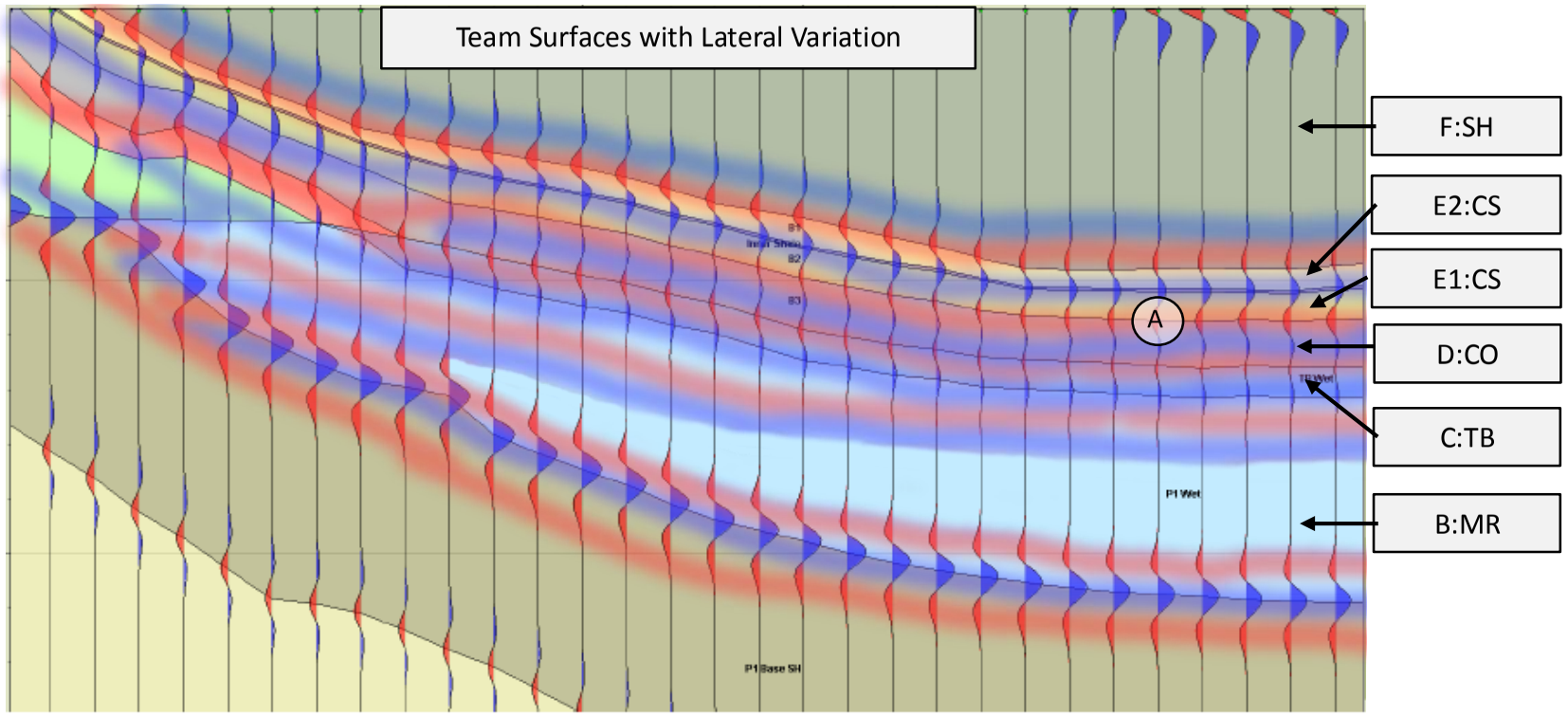


*Figure 39: Zoom view of Model Surfaces with lateral variation, with synthetics and sketch seismic overlay.*

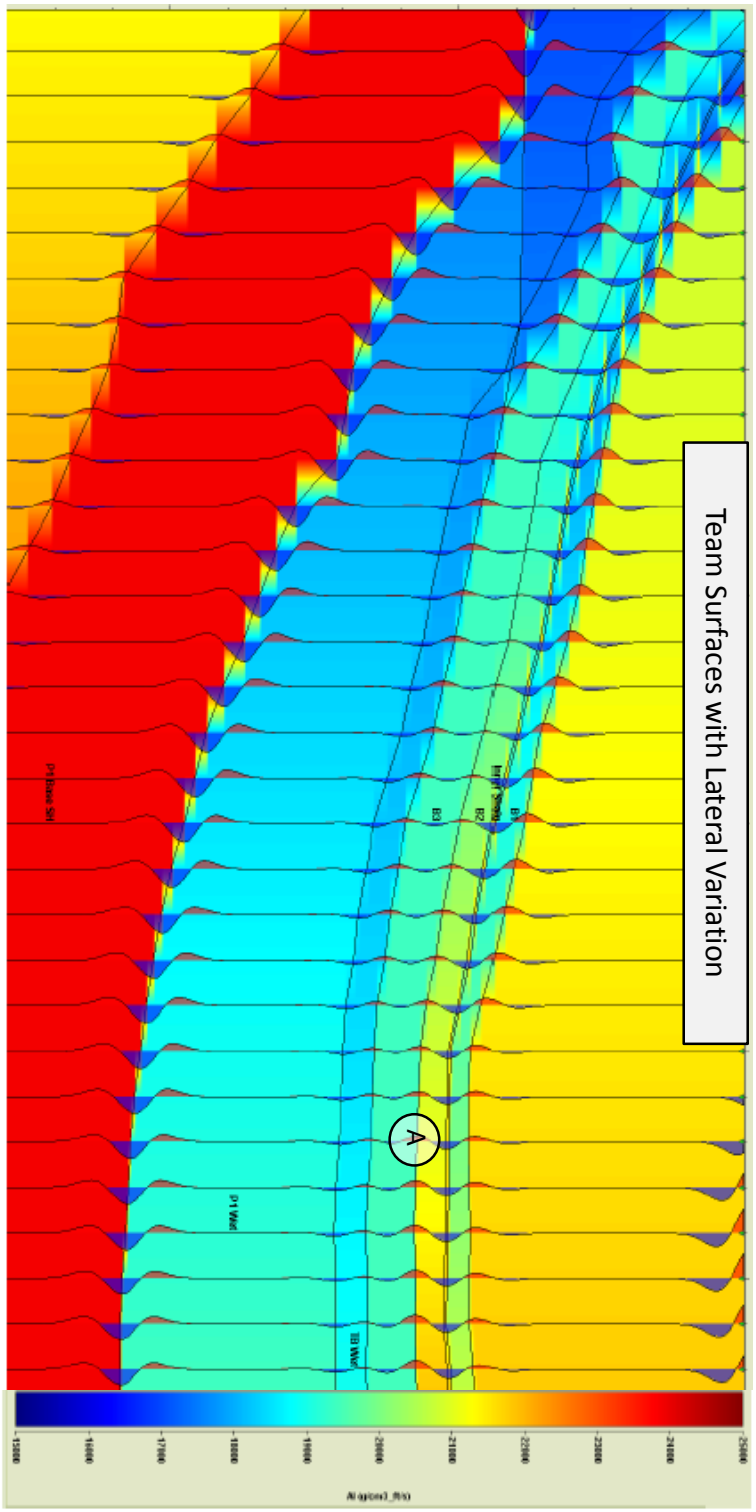


*Figure 40: Zoom view of Model Surfaces with lateral variation, relative impedances.*

## Tables

*Table 1: Velocity and density values used in initial RokDoc models*

| Model Fills | | Fluid | V_p (ft/s) | Density (g/cm$^3$) |
|---|---|---|---|---|
| Salt | | | 15000 | 2.15 |
| F:SH | Shale | | 9200 | 2.35 |
| E2:CS | Channel Sands | Water Sand | 8600 | 2.15 |
| Inner Shale | | | 9200 | 2.35 |
| E1:CS | Channel Sands | Water Sand | 8600 | 2.15 |
| Sand Pulse | | Water Sand | 8600 | 2.15 |
| D:CO | Cut Off | | 9200 | 2.35 |
| C:TB | Thin Beds | Oil Sand | 8000 | 2.2 |
| C:TB | Thin Beds | Water Sand | 9000 | 2.27 |
| B:MR | Main Reservoir | Oil Sand | 7500 | 2.08 |
| B:MR | Main Reservoir | Water Sand | 8600 | 2.15 |
| Base Shale | | | 9300 | 2.35 |

## Appendix

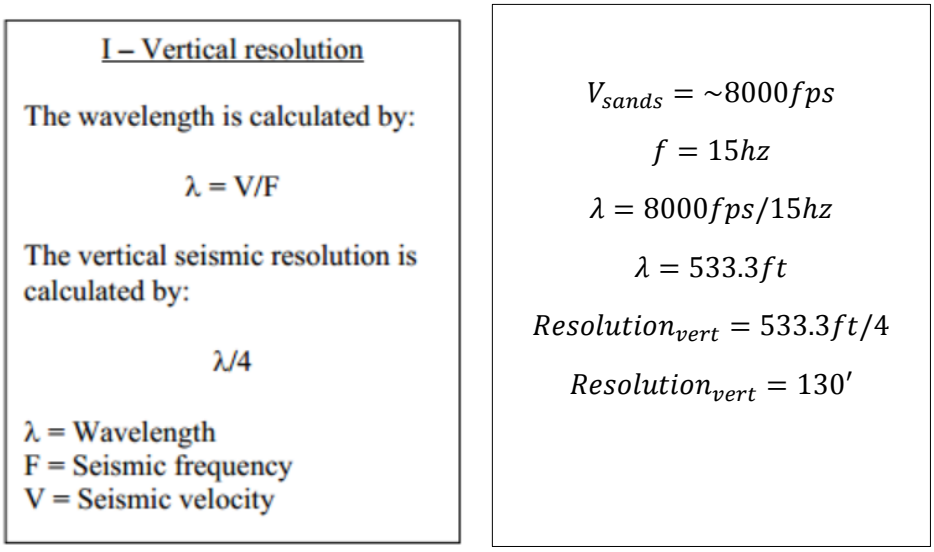

I – Vertical resolution

The wavelength is calculated by:

$\lambda = V/F$

The vertical seismic resolution is calculated by:

$\lambda/4$

$\lambda$ = Wavelength
F = Seismic frequency
V = Seismic velocity

$$V_{sands} = \sim 8000 fps$$

$$f = 15hz$$

$$\lambda = 8000 fps / 15hz$$

$$\lambda = 533.3 ft$$

$$Resolution_{vert} = 533.3 ft/4$$

$$Resolution_{vert} = 130'$$

*Equation 1: Vertical seismic resolution calculation, Rafaelsen, 2014.*

*Table 2: Body values for lateral variation model.*

| Fills used in Lateral Variation With Model Surfaces | | | | | | | |
|---|---|---|---|---|---|---|---|
| | | | V_p (ft/s) | | | Density ($g/cm^3$) | |
| | | Trace | 8 | 52 | | 8 | 52 |
| Salt | | | 15000 | | | 2.15 | |
| F:SH | Shale | | 8790 | 9290 | | 2.31 | 2.36 |
| E2:CS | Channel Sands | | 7420 | 9180 | | 2.11 | 2.31 |
| Inner Shale | | | 9200 | | | 2.35 | |
| E1:CS | Channel Sands | | 7930 | 9750 | | 2.11 | 2.29 |
| D:CO | Cut Off | | 8650 | 8900 | | 2.27 | 2.25 |
| C:TB | Thin Beds | | 7670 | 8010 | | 2.14 | 2.17 |
| C:TB | Thin Beds | | 8010 | 9000 | | 2.15 | 2.24 |
| B:MR | Main Reservior | | 7710 | 8130 | | 2.11 | 2.15 |
| B:MR | Main Reservior | | 8130 | 9000 | | 2.15 | 2.25 |
| Base Shale | | | 10000 | | | 2.39 | |